Quantum states of cylindrical surface charge density for modeling plasmonic circuit elements: Nanowires, nanorods, cavities, and waveguides

M. Bagherian [1,*] and A. Passian [2,†]

[1] *Department of Computational Medicine and Bioinformatics, University of Michigan, Ann Arbor, Michigan 48109, USA*

[2] *Quantum Information Science, Oak Ridge National Laboratory, Oak Ridge, Tennessee 37831-6123, USA*

(Received 4 January 2022; accepted 19 May 2022; published 6 June 2022)

Nanostructures in the form of ellipsoids, prolate spheroids, rings, and cylinders are known to exhibit resonant surface and cavity modes with applications in nanophotonics and plasmonics and, more recently, in novel quantum experiments, in which control of plasmons and their interactions with plasmons, photons, phonons, excitons, and quantum emitters are desired. Nanorods and nanowires are examples of plasmonic structures with spectral properties of potential use as interconnects and circuit components. Estimates of the surface properties of these components are needed in circuit design and integrated systems. Here, we present a quantum Hamiltonian for the cylindrical surface charge density. We then study the photon excitation of plasmons on the cylindrical surface and calculate their scattering and radiative decay rate. Nonradiative decay of plasmons induces an efficient heating of the nanoparticle and can photoacoustically excite mechanical oscillations. Computational calculations are also presented for the plasmonic modes and the ensuing excitations of nanomechanical eigenmodes of nanoparticles with near-cylindrical symmetries.

DOI: 10.1103/PhysRevA.105.063507

I. INTRODUCTION

Large-aspect-ratio metal and semiconductor structures, such as wires and antennas, owing to their superior transport properties, have enabled conduction of energy and information across device-relevant and free-space length scales, enabling electronics and communication. Collective electronic effects in the surface regions of metal nanoparticles with various morphologies have enabled plasmonics [1]. Mixed photon-surface mode excitations have enabled polaritonics, where hybrid particles composed of photons are strongly coupled to surface modes or quasiparticles (e.g., plasmons, excitons) and can carry information. Much opportunity awaits such structures to enable novel effects in these contexts and beyond in topological and quantum materials and in quantum sensing. Examples are numerous in the range from conceptual designs, such as ion and molecular trapping in nanorings [2] to experimentally demonstrated cases, such as plasmon-assisted electron emission from nanotips [3]. Exotic states such as the formation of topological solitons or twistons [4] in graphene nanoribbons and bendons [5] in nanowires are other examples.

In the limit of very large aspect ratio, the cylindrical system approaches a one-dimensional (1D) material, which has the potential to enable new capabilities in electronics and computing [6]. Examples include use of carbon nanotubes as the gate materials in transistors to overcome the beyond-Moore-law development [6] and the topological states in emerging computing paradigms [6]. Nanoscale cylindrical domains occupied by a single material or multiple materials, as in the case of Janus arrangement or a stratified medium [7,8], offer unique prospects for emerging quantum circuits and devices, where low-loss fast surface mode dynamics may facilitate qubit manipulations and operations.

It is known that photon-surface plasmon interactions, similar to photon-atom interactions, lead to elastic and inelastic scattering. Therefore, many scattering processes such as Raman, Compton, Thomson, and Rayleigh that lead to emission and absorption may be treated if the needed surface plasmon operators can be constructed. Field enhancement and coherent oscillations as a result of plasmon excitation are accompanied by thermal effects due to nonradiative decay of plasmons [9–11]. Recent theoretical calculation suggests the entanglement of a pair of qubits subject to a dissipative plasmonic reservoir [12]. Moreover, theoretical study of the electromagnetic field imbalance in surface plasmon polaritons (SPPs) [13–15], and interaction of a single photon with two-level quantum dots [16] have been discussed.

A segment of a conceptual circuit component depicting use of quantum surface modes is shown in Fig. 1. The extended dimension along the cylindrical axis, and the cross-sectional dimensions similar to finite-volume nanoparticles, calls for specific attention when modeling the electronic and optical responses. Particles with genus g surfaces, appear very promising for both classical and quantum sensing, but the value of g can significantly alter the accessibility and tractability of analytical solutions. For $g = 0$, one obtains a sphere, for which much work has been reported (Mie theory). Recently, we reported quantum calculations for infinite geometries [17] and both classical and quantum calculations and the added analytical complexity for particles with $g = 1$, which generates a torus [18].

*bmaryam@umich.edu

†passianan@ornl.gov

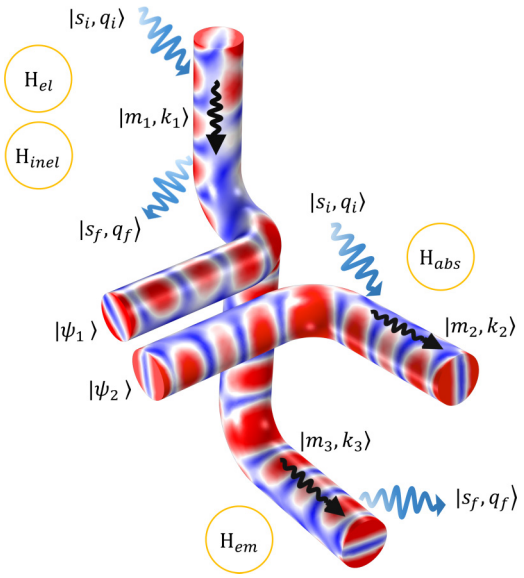

FIG. 1. A segment of a conceptual circuit in plasmonics implemented using cylindrical and toroidal subunits for transport of information. Analogous to electronic circuitry, plasmonic circuits may be envisioned to be intimately integrated with nanophotonics in which information is transported by utilizing fast electronic excitations in a variety of nanostructures. Here, the eigenmodes of surface charge density, making up the quantum states, may be approximated by $|m_i, k_i\rangle$ cylindrical states. New quantum states $|\Psi_i\rangle$ emerging out of the interaction region are envisioned to take the form of correlated cylindrical plasmonic eigenstates. In elastic scattering ($H_{\rm el}$), photons (blue arrows) are scattered into a cone of directions at an angle about the cylindrical axis, while in inelastic scattering ($H_{\rm inel}$) a plasmon (black arrows) is excited. Absorption ($H_{\rm abs}$) entails a photon being annihilated to create a plasmon, while in emission ($H_{\rm em}$), a plasmon is annihilated to create a photon.

The axial resonance properties of the cylindrical surface modes are wavelength λ dependent, the strength of which is affected by the length z_C of the cylindrical structure. The corresponding frequencies ω of the axial surface charge density oscillations can thus vary for a cylindrical particle of radius r_C when $z_C \propto r_C$, versus when $z_C \gg r_C$. Furthermore, unlike atomic systems with sharp and distinct resonances, nanoparticles possess elaborate spectral features and plasmon dispersion relations, which are strongly material dependent. In this article, we present a quantum Hamiltonian for a cylindrical nanostructure such that the underlying normal mode distribution associated with the surface charge density can be illuminated. As applications of the Hamiltonian, we employ Ritchie's interaction Hamiltonian [19] and calculate the radiative decay, followed by absorption, elastic, and inelastic scattering of cylindrical surface plasmons. In doing so, we first calculate the plasmon dispersion relations for cylindrical media. For appropriate values of r_C, the dispersion relations agree well with the quasistatic plasmon dispersion, which will also be discussed.

The presentation has been organized as follows. In Sec. II, we introduce the modeled system and calculate the plasmon dispersion relations. Here, we show the recovery of the quasistatic dispersion relations in suitable limits. This section ends with computational results to account for the nonradiative decay of plasmons and the photothermal excitation of mechanical motion. In Sec. III, we first calculate the noninteracting quantum Hamiltonian for a solid cylinder in vacuum. We then calculate the interaction of photons with surface plasmons for the cylindrical electronic system. Therefore, in Sec. VI, we begin to set up the photon and surface plasmon operators. Cross sections and transition probabilities, involving appropriate matrix elements, for photons interacting with cylindrical surface plasmons, will follow. Our work closely follows the approach by Ritchie *et al.* (see, e.g., Ref. [18]). Lastly, we conclude in Sec. VII.

II. DISPERSION AND FIELDS OF CYLINDRICAL SURFACE PLASMONS

The interaction of the radiation field with matter, described as a scattering process, may exhibit strong spectral variation depending upon the geometric and material properties. Therefore, prior to quantization of the cylindrical surface waves to obtain the surface plasmon states, we consider electromagnetic normal modes of the solid domain as a starting point. With reference to Appendix B, solving the Helmholtz equation for points $\mathbf{r} = (\rho, \varphi, z)$ in a domain partitioned by an infinite cylinder of radius $\rho = \rho_0$, the solution set of eigenfunctions is given in terms of modified Bessel functions of first and second kinds, $I_m(\kappa\rho)$ and $K_m(\kappa\rho)$, respectively, for the triple (κ, k_z, m), where the choice of Bessel functions depends on two factors: (1) the radiative or nonradiative regime being considered and (2) the asymptotic behavior of the modified Bessel functions. Therefore, in the nonradiative regime, the solutions may be obtained for the z component of the electric field as

$$E_z(\mathbf{r}, t) = \sum_{m=-\infty}^{\infty} \mathscr{C}_m(t) e^{i(k_z z + m\varphi - \omega t)} [\theta_m^<(\kappa_{\rm i}, \rho) + \theta_m^>(\kappa_{\rm o}, \rho)], \tag{1}$$

where $\mathscr{C}_m(t)$ is the complex mode amplitude at time t, with $m \in \mathbb{Z}$, counting the azimuthal modes, where we introduce

$$\theta_m^<(\kappa, \rho) = \Theta(\rho_0 - \rho)\, I_m(\kappa\,\rho)\, K_m(\kappa\,\rho_0), \tag{2}$$

$$\theta_m^>(\kappa, \rho) = \Theta(\rho - \rho_0)\, I_m(\kappa\,\rho_0)\, K_m(\kappa\,\rho), \tag{3}$$

after partitioning the space with the Heaviside function Θ, with the half-maximum convention, $\Theta(0) = 1/2$.

Denoting the dielectric functions at frequency ω for the interior and exterior domains by $\varepsilon_{\rm i}$ and $\varepsilon_{\rm o}$, we impose Dirichlet and Neumann boundary conditions [see Eq. (B7)]. Considering the dielectric properties of the involved media $\varepsilon_{\rm i}/\varepsilon_{\rm o}$, we may assume $\varepsilon_{\rm o} = 1$ and $\varepsilon_{\rm i}(\omega) = \varepsilon(\omega)$, that is a vacuum-bounded solid cylinder with a local frequency-dependent dielectric function. Therefore, one may obtain

$$\varepsilon(\omega) = \frac{\kappa_{\rm i}^3\,\kappa_{\rm o}^3\,\mathcal{I}_m\,\mathcal{K}_m - \kappa_{\rm i}^4\,\kappa_{\rm o}^2\,\mathcal{K}_m^2 + (m\omega_p k_z/\rho_0)^2}{\kappa_{\rm i}^2\,\kappa_{\rm o}^4\,\mathcal{I}_m^2 - \kappa_{\rm i}^3\,\kappa_{\rm o}^3\,\mathcal{I}_m\,\mathcal{K}_m + (m\omega_p k_z/\rho_0)^2}, \tag{4}$$

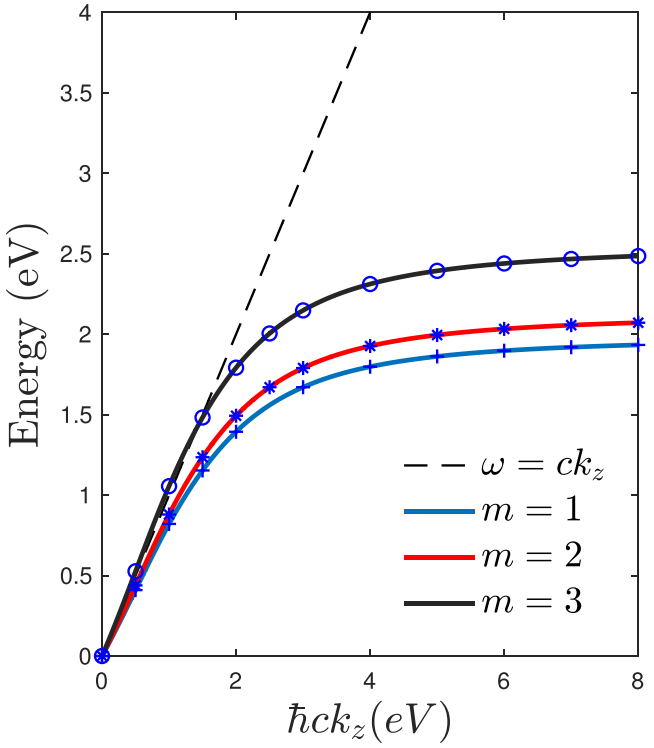

FIG. 2. Energy dispersion of the first three surface plasmon modes excited on a cylinder of radius $\rho = 50$ nm. The cylindrical domain is modeled as a Drude material (see Appendix A) bounded by vacuum.

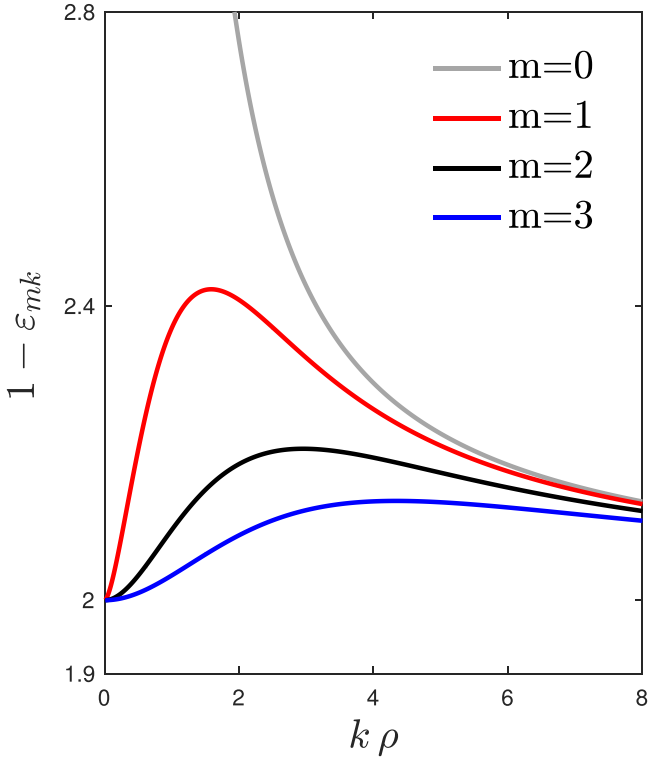

FIG. 3. Quasistatic resonance values of the dielectric function for the first few leading modes. The cylindrical domain is modeled as a free electron gas bounded by vacuum, that is, the y axis is ω_p^2/ω^2.

where

$$\mathcal{I}_m = \left[\frac{d}{d(\kappa_i \rho)} \ln I_m(\kappa_i \rho)\right]\Big|_{\rho=\rho_0}, \tag{5}$$

$$\mathcal{K}_m = \left[\frac{d}{d(\kappa_o \rho)} \ln K_m(\kappa_o \rho)\right]\Big|_{\rho=\rho_0}, \tag{6}$$

for $m = 0, 1, 2, \ldots$ (also see Ref. [20]).

The energies of the first few plasmon modes m in Fig. 2 [obtained by solving Eq. (B10) explicitly for ε] correspond to set of pairs (k_z, ω) for which Eq. (B10) is zero, that is, for each m, the roots (k_z, ω) of the implicit function Eq. (B10) are found and enhanced by interpolation. The results agree well with reported cylindrical surface modes [8,21]. The solutions on the right-hand side of the light line $\omega = c\,k_z$ correspond to the nonradiative regime (whereas the radiative regime solutions will appear on the left-hand side, not displayed).

The quasistatic plasmon dispersion relations may be obtained from Eq. (B10) by letting $c \to \infty$. Alternatively, they may also be obtained directly from the scalar potentials satisfying the Laplace equation, as described in Appendix C, where we have shown that our solution in Eq. (B10) agrees well with the special case of that of a multilayered cylinder [8]. In the quasistatic limit, we note from the scalar electric potential (see Appendix D),

$$\Phi(\mathbf{r}, t) = \sum_{m=-\infty}^{\infty} \int_{-\infty}^{\infty} C_{mk}(t) e^{i(m\varphi + kz)} \times [\theta_m^<(|k|, \rho) + \theta_m^>(|k|, \rho)]\, dk, \tag{7}$$

that the amplitudes satisfy $C_{mk}(t) = \overline{C_{-m-k}}(t)$, using the fact that the scalar potential is real-valued (see Appendix D). Following Eqs. (D7)–(D13), the equation of motion for the surface charge will now take the form $\ddot{C}_{mk}(t) + \omega_{mk}^2 C_{mk}(t) = 0$, where

$$\omega_{mk}^2 = \omega_p^2\, |k|\, \rho_0\, I_m'(|k|\rho_0)\, K_m(|k|\rho_0) \tag{8}$$

are found to be equal to those obtained above and shown in Fig. 3.

The effect of retardation on the surface plasmon energies may now be explicitly investigated for each mode of a given cylinder. For $m = 1, 2, 3$ and $\rho = 50$ nm, Fig. 4 compares the solutions of Eqs. (4) and (8). Similar to Cartesian surface modes, the quasistatic mode energies are red shifted by the retardation to be completely confined to the region below the light line. In many cases, the differences in the dispersion relations are smaller when comparing the retarded versus quasistatic solutions. In the simpler case of the Cartesian solutions, for example, this is observed by all the dispersion branches being pushed down below the light line when one accounts for retardation.

Having obtained the surface plasmon dispersion relations, one may now consider a specific example to illuminate the calculation of the plasmon fields and photothermal effects. Plasmon decay, in addition to radiative processes, generates substantial heat. Beyond presenting a quantitative assessment of the nonradiative losses, here the effect does not play a significant role (unless one attempts plasmon sensing or surface-enhanced Raman spectroscopy or imaging). However,

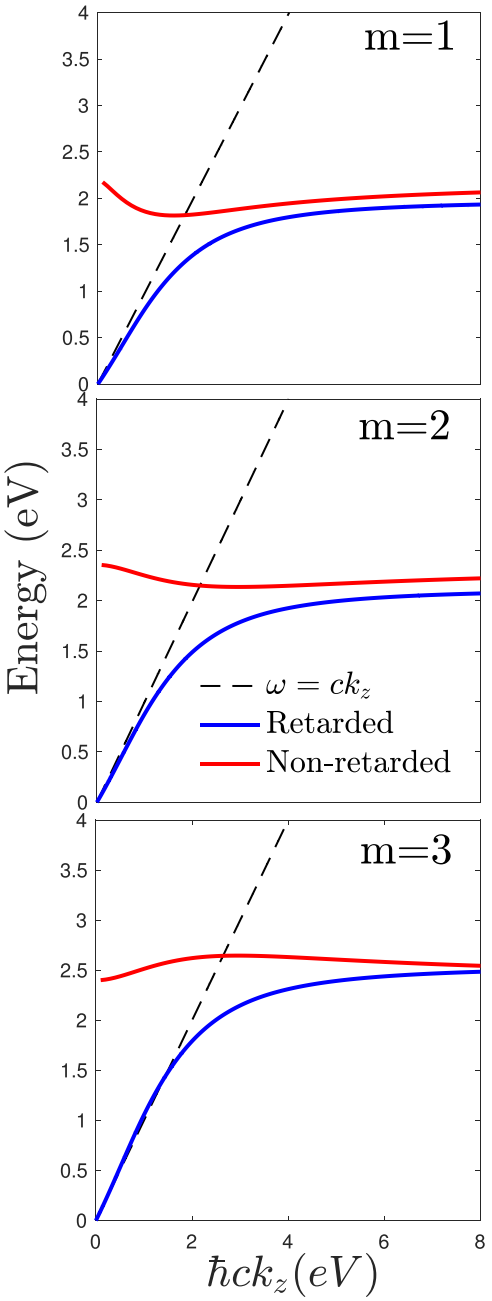

FIG. 4. Effect of retardation on the surface plasmon dispersion. A comparison between quasistatic dispersion relations given in Eq. (B10) and the quasistatic limit given in Eq. (8) for fixed modes $m = 1, 2, 3$ and for a fixed $\rho = 50$ (nm) has been shown. In each plot, the dashed line represents the light line $\omega = ck_z$, while solid blue line is obtained using Eq. (B10) and as described in Fig. 2. Lastly, solid red line is the energy levels obtained for different values of frequency given by Eq. (8).

the effect is not only significant but must indeed be included in the calculations for proper assessment of, for example, Raman cross section calculations of the surface enhancement. The term "thermoplasmonics" was introduced in Ref. [22] to emphasize the photothermal nature and processes associated with plasmon resonances. As an example, we further discuss these points using the specific example of a nanorod, as described in Appendix A.

III. HAMILTONIAN OF THE SURFACE CHARGE DENSITY

The initial state of the system may be composed of the initial state of the cylindrical surface plasmon and the initial state of an incident photon. This initial state may then transition into a state composed of the final states of the plasmon and an outgoing particle. To calculate the scattering rate, that is, the rate of transitions in these events, we will require the plasmon Hamiltonian in terms of creation and annihilation operators. With the canonical form obtained, other related operators can be constructed. In addition, having a quantum Hamiltonian that explicitly shows the eigenmodes is helpful for analyzing the various transitions or when calculating other quantum scenarios, for example, qubit-plasmon coupling for quantum information processing or performing quantum optical operations such as quantum-dot-induced beam splitting [16]. In general, when treating, for example, the coupling between a quantum emitter and a plasmonic nanostructure, having an appropriate quantum Hamiltonian for the nanostructure is necessary for the calculations. Other potentially important information includes the development of concepts based on entangled plasmons, entangled photon-plasmon, plasmon-electron, etc. In all such calculation, utilizing specific quantum states of the plasmonic system could be beneficial. Electronically large systems such as various nanoparticles pose difficulty for many-body treatments that take into account the geometry of the electronic system. The presented treatment helps illuminate the inner working of involved quantum modes.

From the potential in Eq. (7), the classical energy E of the cylindrical polarization surface charges can be calculated (Appendix E) for a scaling factor b as

$$E = \frac{b\pi}{2} \sum_{m=-\infty}^{\infty} \int_{-\infty}^{\infty} \frac{\theta_m(k, \rho_0)}{\omega_{mk}^2} [|\dot{C}_{mk}(t)|^2 + \omega_{mk}^2 |C_{mk}(t)|^2]\, dk, \tag{9}$$

where, for convenience, we have defined

$$\theta_m(k, \rho_0) = I_m(|k|\rho_0) K_m(|k|\rho_0).$$

Following the symmetry properties of modified Bessel functions and the relations outlined through Eqs. (E7)–(F9), we write the amplitudes in terms of the new complex functions c_{mk} as

$$C_{mk}(t) = \frac{\gamma_{mk}}{2\omega_{mk}} [c_{mk}(t) + c^*_{-m-k}(t)], \tag{10}$$

$$\dot{C}_{mk}(t) = \frac{i\gamma_{mk}}{2} [c_{mk}(t) - c^*_{-m-k}(t)], \tag{11}$$

and thus express the energy as

$$E = \frac{b\pi}{4} \sum_{m=-\infty}^{\infty} \int_{-\infty}^{\infty} \frac{\gamma_{mk}^2}{\omega_{mk}^2} \theta_m(k, \rho_0)(c_{mk} c^*_{-m-k} + c^*_{mk} c_{-m-k})\, dk \tag{12}$$

using

$$|\dot{C}_{mk}(t)|^2 + \omega_{mk}^2 |C_{mk}(t)|^2 = \frac{\gamma_{mk}^2}{2} (c_{mk} c^*_{-m-k} + c^*_{mk} c_{-m-k}).$$

We can now write (12) as a quantum Hamiltonian in terms of the annihilation and creation operators, $\hat{c}_{mk}$ and $\hat{c}^\dagger_{mk}$,

respectively,

$$H = \frac{1}{2}\sum_m \int_{-\infty}^{\infty} \hbar\omega_{mk}\,(\hat{c}^{\dagger}_{mk}\hat{c}_{mk} + \hat{c}_{mk}\hat{c}^{\dagger}_{mk})\,dk. \tag{13}$$

From the equity of Eqs. (9) and (13) while using Eqs. (10) and (11), one finds

$$\gamma^2_{mk} = \frac{2\hbar}{b\pi}\frac{\omega^3_{mk}}{\theta_m(k,\rho_0)}. \tag{14}$$

To obtain the quantized scalar potentials, we consider $\Phi_{\rm i}$ given by Eq. (7) for $\rho_0 < \rho$ and its complex conjugate. Following Appendix F, using the fact that the scalar potential is real valued, and Eq. (14), we obtain the following complex amplitudes:

$$C_{mk}(t) = \sqrt{\hbar}\,A_{mk}(\hat{c}_{mk} + \hat{c}^{\dagger}_{-m-k}),$$

with

$$A_{mk} = \sqrt{\frac{\hbar\omega_{mk}}{2b\pi\theta_m(k,\rho_0)}}, \tag{15}$$

where the operator c_{mk} and its complex conjugate c^*_{mk} are replaced by creation and annihilation operators, $\hat{c}_{mk}$ and $\hat{c}^{\dagger}_{mk}$, respectively. Therefore, Eq. (7) can be rewritten as

$$\Phi(\mathbf{r},t) = \sum_{m=-\infty}^{\infty}\int_{-\infty}^{\infty} A_{mk}[\theta^{<}_m(|k|,\rho) + \theta^{>}_m(|k|,\rho)] \times (\hat{c}_{mk} + \hat{c}^{\dagger}_{-m-k})e^{i(kz+m\varphi)}\,dk,$$

with $\theta^{<}_m$ and $\theta^{>}_m$ given in Eqs. (2) and (3). In order to transit from integral to sum, one may use a quantization volume $\mathcal{V}$, enclosing a length $\mathcal{L}$ of the cylinder, where $\mathcal{V} = \pi\rho_0^2\mathcal{L}$. Carrying the integral to a sum, where in transition, we have utilized the expression [23] $\sum_k \to \sqrt{\frac{\mathcal{L}}{2\pi}}\int dk$, the quantized potential is found:

$$\Phi(\mathbf{r},t) = \sqrt{\frac{2\pi}{\mathcal{L}}}\sum_{m=-\infty}^{\infty}\sum_k A_{mk}\,[\theta^{<}_m(|k|,\rho) + \theta^{>}_m(|k|,\rho)] \times (\hat{c}_{mk} + \hat{c}^{\dagger}_{-m-k})e^{i(kz+m\varphi)}.$$

It is instructive to note that, utilizing the potential and kinetic energies, given in Eqs. (E5) and (E6), respectively, the Lagrangian of the system takes the explicit form

$$L = \frac{1}{4}\sum_{m=-\infty}^{\infty}\int_{-\infty}^{\infty}\frac{|\dot{C}_{mk}(t)|^2 - \omega^2_{mk}|C_{mk}(t)|^2}{\omega_{mk}\,A^2_{mk}}dk,$$

from which we derive the equation of motion as

$$|\ddot{C}_{mk}(t)|^2 - \omega^2_{mk}|C_{mk}(t)|^2 = 0.$$

Noting the real-valued electric scalar potentials, the amplitudes [see Eq. (F5)] satisfy $C_{mk}(t) = \overline{C_{-m-k}}(t)$, for all m and k. In order to quantize the system, it is convenient to separate the real and imaginary parts of the complex dynamical variables $C_{mk}(t)$ by defining real dynamical variables x_{mk} and y_{mk} and write

$$C_{mk}(t) = x_{mk} + i\,y_{mk}.$$

The Lagrangian now becomes a function of the coordinates x_{mk} and y_{mk} as

$$L = \frac{1}{4}\sum_{m=-\infty}^{\infty}\int_{-\infty}^{\infty}\frac{1}{\omega_{mk}\,A^2_{mk}}\{|\dot{x}_{mk}(t)|^2 - \omega^2_{mk}\,|x_{mk}(t)|^2 + 2i[\dot{x}_{mk}(t)\dot{y}_{mk}(t) - \omega^2_{mk}\,x_{mk}(t)\,y_{mk}(t)] - |\dot{y}_{mk}(t)|^2 - \omega^2_{mk}\,|y_{mk}(t)|^2\}\,dk,$$

and the corresponding "velocities" $\dot{x}_{mk}$ and $\dot{y}_{mk}$ and conjugate momenta ($p_{mk} = \partial L/\partial\dot{x}_{mk}$ and $q_{mk} = \partial L/\partial\dot{y}_{mk}$):

$$p_{mk} = \frac{1}{2}\sum_{m=-\infty}^{\infty}\int_{-\infty}^{\infty}\frac{[\dot{x}_{mk}(t) + i\dot{y}_{mk}(t)]}{\omega_{mk}A^2_{mk}}\,dk, \tag{16}$$

$$q_{mk} = \frac{1}{2}\sum_{m=-\infty}^{\infty}\int_{-\infty}^{\infty}\frac{-[\dot{x}_{mk}(t) + i\dot{y}_{mk}(t)]}{\omega_{mk}A^2_{mk}}\,dk. \tag{17}$$

The Hamiltonian now takes the form

$$H = \sum_{m,k}(p_{mk}\dot{x}_{mk} + q_{mk}\dot{y}_{mk}) - L,$$

and by inverting Eqs. (16) and (17),

$$H = \sum_{m=-\infty}^{\infty}\int_{-\infty}^{\infty}\frac{1}{\omega_{mk}\,A^2_{mk}}[|\dot{x}_{mk}(t) + i\,\dot{y}_{mk}(t)|^2 + \omega^2_{mk}\,|x_{mk}(t) + i\,y_{mk}(t)|^2]\,dk,$$

which gives

$$H = \frac{b\pi}{2}\sum_{m=-\infty}^{\infty}\int_{-\infty}^{\infty}dk\,\theta_m(k,\rho_0)\Big[|x_{mk}(t) + i\,y_{mk}(t)|^2 + \frac{1}{\omega^2_{mk}}|\dot{x}_{mk}(t) + i\,\dot{y}_{mk}(t)|^2\Big],$$

and is thus consistent with the classical energy given in Eq. (9).

IV. INTERACTION HAMILTONIAN

Here, we consider the quantum formulations to describe the photon-surface charge interaction, in which the solid cylinder may be treated as an electron fluid. Briefly, without any specific boundary conditions, we may invoke the hydrodynamical formulation of a plasma. The collective linearized hydrodynamic equation of motion for an electron, ignoring the damping, in an electric field is written as

$$\frac{\partial\mathbf{v}}{\partial t} = -\frac{e}{m}\,\mathbf{E} - \frac{\beta^2}{n_0}\nabla n_1(\mathbf{r},t), \tag{18}$$

where $\mathbf{v}$ denotes the nonequilibrium velocity correction to the static sea of electrons, β is the propagation speed of the disturbance through the electron gas, and $\nabla n_1(\mathbf{r},t)$ denotes the semiclassical correction term in electron charge density, that is,

$$n(\mathbf{r},t) = n_0 + n_1(\mathbf{r},t),$$

while n_0 is the electronic density in the undisturbed state satisfying $n_1 \ll n_0$. The last term in Eq. (18), originates from a quantum description of pressure effects in the electron

gas. The continuity equation is given as $\partial_t n = -\nabla \cdot (n\mathbf{v})$. In Eq. (18), the first term is the Lorentz force, while the second term is due to the internal kinetic energy of the electron gas, here described within the Thomas-Fermi model, with β proportional to the Fermi velocity $\mathbf{v}_F$ [24,25]. In order to solve Eq. (18) along with the continuity equation, the standard procedure is to expand the physical fields in a zeroth-order static term, where, as mentioned above, n_0 is the homogeneous static electron density, with a small first-order dynamic term, n_1 [26]. In the frequency domain, and by linearizing the equations, one may obtain

$$\beta^2 \nabla(\nabla \cdot \mathbf{J}) + \mathbf{J} = i\frac{e^2 n_0}{m\omega}\mathbf{E},$$

where $\mathbf{J}$ is the induced current density, here, the cylindrical surface charge, which can be written as $\mathbf{J} = -n_0 e\,\mathbf{v}$, where n_0 and e denote the number density of electrons and charge of the electron, respectively [24]. Within the linearized hydrodynamic model using quantization and perturbation theory, Ritchie and Wilems [27] obtained important interaction Hamiltonians. An example is $H^{\text{int}} = \frac{1}{c}\int \mathbf{J}\cdot\mathbf{A}\,d\Omega$, where $\mathbf{A}$ is the vector potential operator of the photon field.

Other interactions of interest include the first and second terms of the perturbed Hamiltonian describing the photon-plasmon interaction, denoted by $H^{\text{int}}_{\text{em}}$ and $H^{\text{int}}_{\text{inel}}$, respectively, in the model developed by Ritchie [19]. The first interaction is useful to describe the creation of a plasmon by a photon (absorption) or the decay of a plasmon into a photon (emission). The second-order interaction describes the inelastic scattering of a photon in creating a plasmon. A zeroth-order interaction $H^{\text{int}}_{\text{el}}$ may be used to describe the elastic scattering of photons due to the presence of an electron gas with uniform density. Thus, with an explicit form of the vector potential operator for the electromagnetic field, $\mathbf{A}$, the various forms of matrix elements of the interaction Hamiltonian may be derived. In what follows, we introduce matrix elements of the main interest and derive the expressions for different kinds of interactions between photons and surface plasmons for a solid cylinder.

To obtain the operator for the current density, we first write the time derivative of the charge displacement vector $\dot{\mathbf{Z}}$ as

$$\dot{\mathbf{Z}} = -\frac{e}{m_e}\nabla \sum_m e^{im\varphi} \times \int_{-\infty}^{\infty} \frac{\dot{C}_{mk}(t)}{\omega_{mk}^2} I_m(|k|\rho) K_m(|k|\rho_0) e^{ikz}\,dk. \tag{19}$$

If we use the following,

$$\dot{C}_{mk}(t) = \frac{i\gamma_{mk}}{2}(\hat{c}_{mk} - \hat{c}^{\dagger}_{-m-k}) = i\sqrt{\hbar}A_{mk}\,(\hat{c}_{mk} - \hat{c}^{\dagger}_{-m-k}),$$

where A_{mk} is given in Eq. (15), then one may write

$$\mathbf{J} = -\frac{i\omega_p^2}{4\pi}\nabla \sum_m \int_{-\infty}^{\infty} \frac{A_{mk}}{\omega_{mk}}(\hat{c}_{mk} - \hat{c}^{\dagger}_{-m-k}) \times I_m(|k|\rho) K_m(|k|\rho_0) e^{ikz} e^{im\varphi}\,dk, \tag{20}$$

where the definition of the bulk plasma frequency $\omega_p = \sqrt{4\pi n_0 e^2/m_e}$ has been used.

Replacing the integral with summation in (20) gives

$$\mathbf{J} = -\frac{i\sqrt{\hbar}\,\omega_p^2}{4\pi\sqrt{b\mathcal{L}}} \sum_m \sum_k \sqrt{\frac{K_m(|k|\rho_0)}{\omega_{mk} I_m(|k|\rho_0)}} \times (\hat{c}_{mk} - \hat{c}^{\dagger}_{-m-k})\,\nabla[I_m(|k|\rho) e^{ikz} e^{im\varphi}]. \tag{21}$$

The current density operator can now be written as $\mathbf{J} = n_0 e\,\nabla\dot{\Psi}$, where $\mathbf{v} = \nabla\dot{\Psi}$, and

$$\dot{\Psi} = \frac{i\sqrt{\hbar}\,\omega_p^2}{4\pi\sqrt{b\mathcal{L}}} \sum_m \sum_k \sqrt{\frac{K_m(|k|\rho_0)}{\omega_{mk} I_m(|k|\rho_0)}} \times (\hat{c}_{mk} - \hat{c}^{\dagger}_{-m-k}) I_m(|k|\rho)\, e^{ikz} e^{im\varphi}. \tag{22}$$

V. PHOTON AND PLASMON STATES

For a photon of wave vector $\mathbf{s}$ and polarization $\hat{\mathbf{e}}_q \perp \mathbf{s}$, $q = 1, 2$, the vector potential, $\mathbf{A}$, in the Coulomb gauge (transversality condition), can be expressed as [28]

$$\mathbf{A} = \frac{c\sqrt{\hbar}}{(2\pi)^3} \sum_{q=1,2} \int \frac{\hat{\mathbf{e}}_q}{\sqrt{\omega_s}} [a_{sq}(t) e^{i\mathbf{s}\cdot\mathbf{r}} + a^*_{sq}(t) e^{-i\mathbf{s}\cdot\mathbf{r}}] d^3 s, \tag{23}$$

where the energy of the photon is given by $\hbar\omega_s$, $\omega_s = cs = c|\mathbf{s}|$ is the photon frequency, and $a_{sq}(t)$ and its conjugate $a^*_{sq}(t)$ are the photon operators, such that the equations for motion of the field for all s are

$$[a_{sq}(t), \dot{a}_{sq}(t)] = (1, -i\omega_s) a_{sq}(0) e^{-i\omega_s t}. \tag{24}$$

To write the photon field as a sum with discrete momentum eigenstates as opposed to the continuous representation, we consider the field to be confined to a volume $\mathcal{V}$, which can be taken to be represented by a cube over which we impose periodic boundary conditions. Since the electromagnetic energy confined to this volume is independent of the shape of the volume [23], we take as our quantization volume as a cylindrical box with volume $\mathcal{V}$ and side $\mathcal{L}$, and carry the following substitutions:

$$\sum_s \to \frac{\mathcal{V}}{(2\pi)^{3/2}} \int d^3 s \to \sqrt{\frac{\mathcal{V}}{(2\pi)^3}} \int d^3 s, \tag{25}$$

where the normalization factor $\frac{1}{\sqrt{\mathcal{V}}}$ [29] has been used to arrive at the last expression. This substitution over the quantization box does not affect the validity of expressions for Hamiltonian and vector potentials [29–31]. Therefore, in second quantization, the vector potential is expressed as

$$\mathbf{A} = \sum_s \sum_{q=1,2} \sqrt{\frac{\hbar c^2}{\mathcal{V}\omega_s}} \hat{\mathbf{e}}_q (\hat{a}_{sq}\, e^{i\mathbf{s}\cdot\mathbf{r}} + \hat{a}^{\dagger}_{sq}\, e^{-i\mathbf{s}\cdot\mathbf{r}}), \tag{26}$$

where $\hat{a}^{\dagger}_{sq}$ and $\hat{a}_{sq}$ denote the creation and annihilation photon operators, respectively, and we write $H_{\mathbf{A}} = \sum_{\mathbf{s},q} \hbar\omega_s\, \hat{a}^{\dagger}_{sq}\hat{a}_{sq}$. A photon in a given momentum and polarization state is written as

$$|\mathbf{s}, q\rangle = \hat{a}^{\dagger}_{sq}|0\rangle, \tag{27}$$

with $|0\rangle$ denoting the zero population in the photon field. The general noninteracting plasmon states including the initial and final states, i and f, respectively, are written as

$$|\sigma\rangle \equiv |\nu_{m_i k_i} \ \dots \ \nu_{m_f k_f}\rangle, \tag{28}$$

where ν_{mk} are the number of plamons in the state (m, k). The quantum state $|\sigma\rangle$ of the cylinder charge density may be written in terms of the number of plasmons in the (m, k) state as $|\nu_{mk}\rangle$, which in the zeroth order is obtained by populating the no-plasmon state $|0\rangle$ via $|\hat{a}^{\dagger}_{mk}|0\rangle$. The plasmon states are orthonormal, that is,

$$\langle \dots \nu_{m_N} \dots \nu_{m_1} | \nu_{k_1} \dots \nu_{k_N} \dots \rangle = \dots \delta_{m_1 k_1} \dots \delta_{m_N k_N} \dots . \tag{29}$$

Similarly, the radiation field in noninteracting state of photons can be represented by

$$|\mathbf{s}, q\rangle \equiv \left|\nu_{s_i q_i} \ \dots \ \nu_{s_f q_f}\right\rangle, \tag{30}$$

where ν_{sq} show the number of photons with wave vector $\mathbf{s}$ and polarization $q = 1, 2$. The general state for the composite photon-plasmon field, using the fact that photon operators act only on the photon states and the plasmon operators only act on plasmons, can be written as

$$|\mathbf{s}, q\rangle \otimes |\sigma\rangle \equiv \left|\nu_{s_i q_i} \ \dots \ \nu_{s_f q_f}\right\rangle \otimes \left|\nu_{m_i k_i} \ \dots \ \nu_{m_f k_f}\right\rangle. \tag{31}$$

In the following calculations, we note that for all photon states sq and $s'q'$, we have

$$\langle 0 \,|\, \hat{a}_{s'q'}\, \hat{a}^{\dagger}_{sq} \,|\, 0\rangle = \delta(s - s')\, \delta_{qq'}, \tag{32}$$

with $\delta(s - s')$ as the Dirac delta function, not to be confused by $\delta_{qq'}$ as the Kronecker delta function. Similarly, for all the plasmon states, mk and $m'k'$, we have $\langle 0 \,|\, \hat{c}_{m'k'}\, \hat{c}^{\dagger}_{mk} \,|\, 0\rangle = \delta(k - k')\, \delta_{mk'}$.

VI. SCATTERING CROSS SECTIONS AND DECAY RATE

A. Elastic scattering

To calculate the scattering cross section, that is, the rate of scattering divided by the flux of the incoming particles, we first set our full system as the combined surface plasmon and photon field. Then we consider the ground state or zero population for both plasmon and photon as $|0\rangle$. The cross section per unit length for the scattering process can be obtained by summing up the transition rate over final states. We proceed by calculating the corresponding matrix element for direct scattering (elastic, including the Thomson limit). For scattering of photons out of the incident beam direction

$$\mathcal{M}_{\rm el} := \langle 0 | \hat{a}_{q_f}(s_f)\, H^{\rm int}_{\rm el}\, \hat{a}^{\dagger}_{q_i}(s_i) | 0 \rangle, \tag{33}$$

for a wave vector $\mathbf{s}$ with indices f and i indicating the final and initial states, respectively, and the zeroth term of the interaction Hamiltonian $H^{\rm int}_{\rm el}$ represents the direct scattering:

$$H^{\rm int}_{\rm el} = \frac{n_0 e^2}{2mc^2} \int_{\rho \leqslant \rho_0} \mathbf{A} \cdot \mathbf{A}\, d\mathcal{V}. \tag{34}$$

Therefore, in calculating $H^{\rm int}_{\rm el}$, using Eq. (26), one may write

$$H^{\rm int}_{\rm el} = \frac{n_0 e^2 \hbar}{2m\mathcal{V}\sqrt{\omega_s\, \omega_{s'}}} \int_0^{\infty} \int_0^{2\pi} \int_0^{\rho_0} \sum_{s,q,s',q'} (\hat{a}_{sq}\, e^{i\mathbf{s}\cdot\mathbf{r}} + \hat{a}^{\dagger}_{sq}\, e^{-i\mathbf{s}\cdot\mathbf{r}})(\hat{a}_{s'q'}\, e^{i\mathbf{s}'\cdot\mathbf{r}} + \hat{a}^{\dagger}_{s'q'}\, e^{-i\mathbf{s}'\cdot\mathbf{r}}) \times (\hat{\mathbf{e}}_q \cdot \hat{\mathbf{e}}_{q'}) h_\rho h_\varphi h_z\, d\rho d\varphi dz. \tag{35}$$

Direct scattering matrix element as expressed in Eq. (33) can now be calculated by means of the commutative relations $[\hat{a}_{sq}, \hat{a}^{\dagger}_{sq}] = \delta_{qq'}\delta_{ss'}$. Therefore,

$$\mathcal{M}_{\rm el} = b^2 \frac{n_0 e^2 \hbar}{2m\mathcal{V}\,\omega_s} \int_0^{\infty} \int_0^{2\pi} \int_0^{\rho_0} \rho\, (\hat{\mathbf{e}}_q \cdot \hat{\mathbf{e}}_q) \times (\hat{a}_{sq}\, e^{i\mathbf{s}\cdot\mathbf{r}} + \hat{a}^{\dagger}_{sq}\, e^{-i\mathbf{s}\cdot\mathbf{r}}) d\rho d\varphi dz, \tag{36}$$

with no m and k dependency. In order to calculate the differential scattering cross section per solid angle Ω, one may utilize the transition-rate formula,

$$w_{fi} = \frac{2\pi}{\hbar^2} |\mathcal{M}_{\rm el}|^2\, \delta(\omega_{s_f} - \omega_{s_0}), \tag{37}$$

to find differential scattering cross section as

$$\frac{d\sigma_{\rm el}}{d\Omega_f} = \frac{1}{c} \sum_{q_f} \int \frac{w_{fi}\, \omega^2_{s_f}}{(2\pi c)^3}\, d\omega_{s_f}. \tag{38}$$

The normalized cross section by unit length is obtained by summing the transition rate over final states and normalizing by length $\mathcal{L}$ and $c \sin\psi_0/\mathcal{V}$, where ψ_0 is the angle between a fixed wave s_0 and the cylindrical axis [30]. Thus,

$$\sigma_{\rm el}|_{\rho_0} = \frac{\mathcal{V}}{\mathcal{L}c \sin\psi_0} \frac{2\pi}{\hbar^2} \sum_{q_f} \sum_{s_f} |\mathcal{M}_{\rm el}|^2\, \delta\big(\omega_{s_f} - \omega_{s_0}\big). \tag{39}$$

B. Emission and absorption

It can be observed from Eqs. (40) and (42) that surface plasmons emission and absorption originate from the same dipole transition matrix element and they assume the same magnitude in principle. Therefore, in this case they are reversible in the sense that an emitted photon from such a quantum system should be absorbed by the same system. In general, the reciprocity between emission and absorption occur for many transitions. This is not unlike the electromagnetic reciprocity, time-reversal symmetries, and Kirchhoff's law of thermodynamics for equilibrium systems, which can impose constraints on emission and absorption properties of, for example, antennas in a broad frequency range. The requirement of reciprocity means that the optical antenna transmits and receives fields equally well from the same direction. Breaking the reciprocity is currently the focus of recent work to enable new applications [32].

Here, we provide a detailed calculations the rate at which an excited surface emits lights per solid angle Ω in a cylindrical domain. Based on the argument above, deriving the same expressions for absorption should follow immediately. The matrix elements corresponding to emission via radiative

decay of surface plasmons may be written as

$$\mathcal{M}_{\rm em} := \langle 0|\hat{a}_{q_f}(s_f)\, H_{\rm em}^{\rm int}\, \hat{c}^{\dagger}_{m_i k_i}\,|0\rangle, \tag{40}$$

where

$$H_{\rm em}^{\rm int} = \frac{1}{c}\int \mathbf{J}\cdot\mathbf{A}\, d\mathcal{V}. \tag{41}$$

The term $H_{\rm em}^{\rm int}$ represents the interaction of one photon and one plasmon, which can be used to predict the creation of a plasmon by a photon or the decay of a plasmon into a photon. This term also corresponds to the interaction Hamiltonian used to calculate the rate of absorption. The matrix element for absorption is given by

$$\mathcal{M}_{\rm abs} := \langle 0|\hat{c}_{m_f k_f}\, H_{\rm em}^{\rm int}\, \hat{a}^{\dagger}_{q_i}(s_i)|0\rangle, \tag{42}$$

which is the Hermitian dual to Eq. (40), since it represents the inverse process.

The interaction Hamiltonian, imposing the Coulomb gauge condition $\nabla\cdot\mathbf{A}=0$ and considering the fact that current is confined to the surface of the cylinder, is given by

$$H_{\rm em}^{\rm int} = -\frac{n_0 e}{c}\int_0^{2\pi}\int_0^{\infty}(\dot{\Psi}\mathbf{A}\cdot\hat{\mathbf{e}}_{\rho})h_{\varphi}\, h_z\, d\varphi\, dz, \tag{43}$$

which leads to

$$H_{\rm em}^{\rm int} = \frac{n_0 e^2}{m_0 c}\sum_{\mathbf{s}}\sum_{k=1,2}\sqrt{\frac{\hbar}{\mathcal{V}\omega_s}}(\hat{\mathbf{e}}_{\rho}\cdot\hat{\mathbf{e}}_k) \times (\hat{a}_{\mathbf{s}k}e^{i\mathbf{s}\cdot\mathbf{r}} + \hat{a}^{\dagger}_{\mathbf{s}k}e^{-i\mathbf{s}\cdot\mathbf{r}})\sum_m \mathcal{J}_m^k(\rho_0), \tag{44}$$

where $\mathcal{V}=\pi\rho_0^2\mathcal{L}$ is the volume of the finite cylindrical box with length $\mathcal{L}$, γ is given in (14), and

$$\mathcal{J}_m^k(\rho) = \int_0^{2\pi}\int_{-\mathcal{L}}^{\mathcal{L}}\left\{\int_0^{\infty} K_m(|k|\rho)I_m(|k|\rho)e^{im\varphi}e^{ikz} \times \frac{-iA_{mk}}{\omega_{mk}}(\hat{c}_{mk}-\hat{c}^{\dagger}_{-m-k})dk\right\}h_{\varphi}h_z\, d\varphi dz, \tag{45}$$

Hence, the emission matrix element becomes

$$\mathcal{M}_{\rm em} = -i\frac{n_0 e^2}{m_0}\sqrt{\frac{\hbar}{\mathcal{V}\omega_s}}\frac{A_{mk}}{\omega_{mk}}\theta_m(k,\rho_0)\mathcal{I}_{mk}(\rho), \tag{46}$$

where

$$\mathcal{I}_{mk}(\rho) = \int_0^{2\pi}\int_{-\mathcal{L}}^{\mathcal{L}}(\hat{\mathbf{e}}_{\rho}\cdot\hat{\mathbf{e}}_k)e^{-i\mathbf{s}\cdot\mathbf{r}}e^{im\varphi}e^{ikz}h_{\varphi}h_z\, d\varphi dz. \tag{47}$$

Taking $\mathbf{s}=\omega_s(\cos\psi, 0, \sin\psi)$, allows us to take $\hat{\mathbf{e}}_q$, as $\hat{\mathbf{e}}_1=(0,1,0)$ and $\hat{\mathbf{e}}_2=(\sin\psi, 0, -\cos\psi)$. This leaves us with two different integrals to calculate:

$$\mathcal{I}_{mk}^{(1)} = b\rho_0\int_0^{2\pi}\int_{-\mathcal{L}}^{\mathcal{L}}\sin\varphi e^{im\varphi}e^{ikz}E_{mk}(\varphi,z)\, d\varphi dz \tag{48}$$

and

$$\mathcal{I}_{mk}^{(2)} = b\rho_0\int_0^{2\pi}\int_{-\mathcal{L}}^{\mathcal{L}}\sin\psi\cos\varphi e^{im\varphi}e^{ikz}E_{mk}(\varphi,z)\, d\varphi dz, \tag{49}$$

where

$$E_{mk}(\varphi,z) = e^{-i\omega_s(\rho_0\cos\psi\cos\varphi+\sin\psi z)}. \tag{50}$$

Radiative decay rate with respect to solid angle Ω is given by the following, which after using (14) takes the form

$$\frac{d\gamma_{mk}}{d\Omega} = \left(\frac{n_0 e^2}{m_e}\right)^2\frac{\theta_m(k,\rho_0)}{8\pi bc^3}\left[\left(\mathcal{I}_{mk}^{(1)}\right)^2 + \left(\mathcal{I}_{mk}^{(2)}\right)^2\right]. \tag{51}$$

The analytic solution for $\mathcal{I}_{mk}^{(1)}$ and $\mathcal{I}_{mk}^{(2)}$ can be obtained as

$$\mathcal{I}_{mk}^{(1)} = \frac{-2ib\rho_0}{\alpha\,\beta}\sin(\mathcal{L}\alpha)\left[(-1)^m e^{-i\beta} - \frac{im}{2\pi}J_m(\beta)\right] \tag{52}$$

and

$$\mathcal{I}_{mk}^{(2)} = \frac{2b\rho_0\sin\psi}{4\pi\alpha}\sin(\mathcal{L}\alpha)\left[J_{m+1}(\beta)+J_{m-1}(\beta)\right], \tag{53}$$

where

$$\alpha = k-\omega_s\,\sin\psi, \quad \beta = \rho_0\,\omega_s\,\cos\psi. \tag{54}$$

In Fig. 5, contour plots corresponding to two specified modes $(m,k)=(0,1)$ and $(m,k)=(0,2)$ for shape parameters ρ, using Eq. (51) and the integral solutions given in Eqs. (52) and (53), are illustrated.

C. Total elastic and inelastic scattering

Matrix element for the total elastic scattering, assuming that γ is the plasmon damping factor, is obtained as shown below:

$$\mathcal{M}_{\rm tel} = \mathcal{M}_{\rm el} + \sum_{mk}\frac{1}{\hbar}\left[\frac{\mathcal{M}_{\rm em}\mathcal{M}_{\rm abs}}{\omega_{s_i}-\omega_{mk}+(i\gamma/2)} - \frac{\mathcal{M}^*_{\rm em}\mathcal{M}^*_{abs}}{\omega_{s_f}+\omega_{mk}-(i\gamma/2)}\right]. \tag{55}$$

For inelastic photon scattering resulting in excitation of a surface plasmon mode (m,k) on the cylinder, the matrix element is

$$\mathcal{M}_{\rm inel} = \langle 0|\hat{a}_{q_f}(s_f)\hat{c}_{m_f k_f}\, H_{\rm inel}^{\rm int}\,\hat{a}^{\dagger}_{q_i}(s_i)|0\rangle, \tag{56}$$

where

$$H_{\rm inel}^{\rm int} = \frac{e^2}{2mc^2}\int \hat{n}(\mathbf{r},t)\,\mathbf{A}\cdot\mathbf{A}\, d\mathcal{V}, \tag{57}$$

with $\hat{n}(\mathbf{r},t)$ being the number charge density operator. The involvement of two photons and one plasmon describes the inelastic scattering of a photon in creating a plasmon. The number density operator $n(\mathbf{r},t)$, is found from the volume charge density, ϱ, for the cylindrical domain. We note Eq. (D1), and with Φ given in Eq. (7), we find

$$\varrho = \frac{\delta(\rho-\rho_0)}{4\pi h_{\rho}^2\rho_0}\sum_{m=-\infty}^{\infty}e^{im\varphi}\int_{-\infty}^{\infty}C_{mk}(t)e^{ikz}\, dk.$$

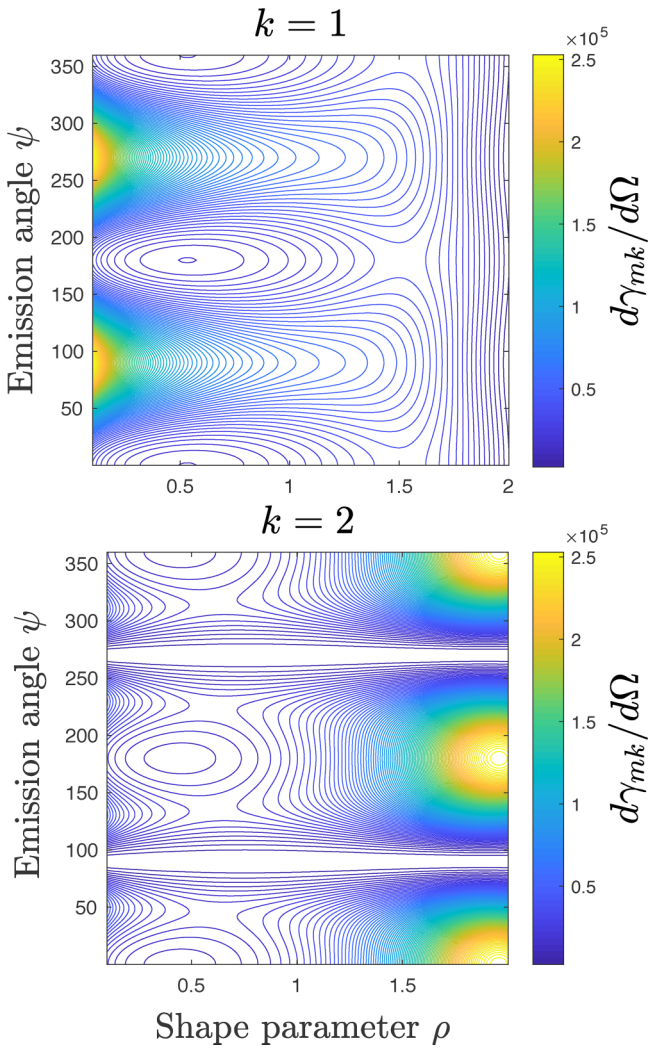

FIG. 5. Contour plots of curvature-induced shift in the radiation pattern associated with the decay of plasmons excited on the cylindrical surfaces for the specified modes $(m, k) = (0, 1)$ (up) and $(m, k) = (0, 2)$ (down), and for different shape parameter ρ and varying emission angle ψ [see Eq. (51)].

Using $C_{mk}(t) = \sqrt{\hbar} A_{mk}(\hat{c}_{mk} + \hat{c}^{\dagger}_{-m-k})$, with A_{mk} given in Eq. (15), the operator $\hat{n}(\mathbf{r}, t)$ can be written as

$$\hat{n}(\mathbf{r}, t) = -\frac{\delta(\rho - \rho_0)}{4\pi\, e\, h_\rho^2 \rho_0} \sum_{m=-\infty}^{\infty} e^{im\varphi} \times \int_{-\infty}^{\infty} \sqrt{\hbar} A_{mk}(\hat{c}_{mk} + \hat{c}^{\dagger}_{-m-k}) e^{ikz}\, dk. \tag{58}$$

Therefore,

$$H_{\text{inel}}^{\text{int}} = -\frac{b\, n_0 e\, \hbar^{3/2}}{8\pi\, m\, \rho_0^2 \mathcal{V} \sqrt{\omega_s\, \omega_{s'}}} \sum_{m=-\infty}^{\infty} \sum_{s,q,s',q'} \int_0^{\infty} \int_0^{2\pi} \int_{-\mathcal{L}}^{\mathcal{L}} \mathcal{G}_m^k(\rho_0)(\hat{\mathbf{e}}_q \cdot \hat{\mathbf{e}}_{q'})(\hat{a}_{sq}\, e^{i\mathbf{s}\cdot\mathbf{r}} + \hat{a}^{\dagger}_{sq}\, e^{-i\mathbf{s}\cdot\mathbf{r}}) \times (\hat{a}_{s'q'}\, e^{i\mathbf{s}'\cdot\mathbf{r}} + \hat{a}^{\dagger}_{s'q'}\, e^{-i\mathbf{s}'\cdot\mathbf{r}}) dz\, d\varphi\, dk, \tag{59}$$

and with $\mathcal{L} \to \infty$, we have

$$\mathcal{G}_m^k(\rho) = A_{mk}(\hat{c}_{mk} + \hat{c}^{\dagger}_{-m-k}) e^{i(m\varphi + kz)}. \tag{60}$$

We may now use Eq. (56) and the commutation relations for photon and plasmons interaction, to obtain the matrix element

$$\mathcal{M}_{\text{inel}} = -\frac{i\, b\, n_0 e\, \hbar^{3/2} \mathcal{L}^{1/2}}{4\pi\, m\, \rho_0^2 \mathcal{V} \sqrt{\omega_s\, \omega_{s'}}} (\hat{\mathbf{e}}_{q_i} \cdot \hat{\mathbf{e}}_{q_f})\, A_{mk}\, J_m(\mu), \tag{61}$$

where $J_m(\cdot)$ denotes the Bessel function of the first kind and μ is calculated by the choice of wave-vector travel direction being perpendicular to the polarization vectors, i.e., $\hat{\mathbf{e}}_q \perp \mathbf{s}$, $q = 1, 2$.

As presented above, by expressing the energy in the canonical form followed by replacing the mode amplitudes with boson creation and annihilation operators for the surface plasmons, various quantum cross sections may be calculated. However, a note on a comparison of these results to classical results may be worthwhile. Despite previous reports [33–35] on the difference between the classical and quantum mechanical definitions of scattering cross sections and the problem of classical limit, the general derivation of classical results from the quantum mechanics, i.e., the reduction theory, is still afar. While such calculations are outside of the current work, to compare the classical and quantum results, one may consider the more tangible case of a finite nanostructure. For example, the prolate spheroidal nanoparticle may be employed in a comparison study.

VII. CONCLUSIONS

In summary, the classical and quantum calculations present a reasonable modeling framework when working with nanostructures with cylindrical symmetry. The quasistatic plasmon dispersion relations, predicting the availability of useful resonance modes in the low-eV range, appear to be modified significantly by retardation effects near the light line. The computed fields, corresponding to the resonance modes, induce significant and rapid (ns) heating of the nanostructures and, by conduction, of the substrate. The quantum calculations, while illustrating the nature of the various surface electronic normal modes, provides a first estimate of the plasmon energies. The obtained Hamiltonian proved useful as a means to calculate relevant scattering quantities. The quantum state of the collective surface charge density oscillation provides a direct access to the quantum numbers of the modes, which can be insightful when studying particle-emitter coupling. In quantum sensing with plasmonic nanostructures, the eigenstates of the Hamiltonian corresponding to different charge oscillations may be useful for coupling to and controlling of specific qubits. It may be of interest to consider specific thin film cylindrical coatings of nonlinear materials, envisioned in a multilayer cylindrical circuit element, which may provide squeezing and entanglement of specific modes. Given the long propagation of surface plasmons, it is conceivable to devise circuits that facilitate transport of qubits across larger segments of an integrated on-chip photonics system. The described photon-plasmon interaction Hamiltonian may be upgraded to a higher order, beyond the first order employed here. The example depicted in Fig. 1, although conceptual, is of current interest in the study of metamaterials, e.g., for designing optomechanical metamaterial systems [36]. Moreover, large-aspect-ratio structures, similar to hyperboloids and paraboloids, are excellent platforms for photoemission,

making the obtained results of potential use for the study of nanostructures as electron sources [37,38]. Similarly, our quantum calculations can serve to further study the electronic and magnetic properties of carbon nanotubes, where cylindrical domains are the natural modeling environment [8,39].

ACKNOWLEDGMENTS

This work was supported in part by the Laboratory Directed Research and Development Program at Oak Ridge National Laboratory (ORNL) under U.S. DOE Grant No. DE-FG2-13ER41967. ORNL is managed by UT-Battelle, LLC, for the U.S. DOE under Contract No. DE-AC05-00OR22725. The U.S. Government retains and the publisher, by accepting the article for publication, acknowledges that the U.S. Government retains a nonexclusive, paid-up, irrevocable, worldwide license to publish or reproduce the published form of this manuscript, or allow others to do so, for U.S. Government purposes.

APPENDIX A: FURTHER DISCUSSIONS ON LOSSES

Here, we present a specific example that illuminates the calculation of the plasmon fields and their photoacoustic or photothermal effects. In the following, to compute the needed fields and spectra, we use the numerical technique of finite elements (FEM [40]). The complex dielectric function $\varepsilon(\omega)$ is taken to be in the Drude form,

$$\varepsilon(\omega) = 1 - \frac{\omega_p^2}{\omega^2 + \Gamma^2} + i\frac{\omega_p^2 \Gamma}{\omega(\omega^2 + \Gamma^2)}, \tag{A1}$$

where ω_p is the usual plasma frequency, and the relaxation constant Γ quantifies the damping. Since the damping is at least three orders of magnitude smaller than the actual energy and its absolute value increases with the increasing k, often one suffices with considering only the real part, as in the case of Fig. 2. We may consider a metallic domain such as a substrate-supported nanoparticle or nanostructure real materials from a comparison with the experimentally determined optical properties of solids (such the compilations by Johnson and Christy [41] or Palik [42]). This configuration is particularly useful for studies of interactions between quantum emitters and the plasmon-supporting particles, as depicted in Fig. 6. As a brief illustration, the dipole-excited fields may be computed, as visualized for the near zone in Fig. 7. For a gold particle immobilized on a quartz substrate, the fields were here computed by numerically solving the 3D field equations subject to appropriate boundary conditions. Assuming a properly polarized incoming field, that is, one which is defined with respect to the symmetries of the structure, we can compute (using the finite elements method) the spectral properties of the ensuing scattering, as shown in Fig. 8. The scattering and extinction cross sections are here given without any normalization (in units m^2 for 3D models). The red shift and significantly lower energy (nW) dissipation for the case with a substrate are evident. With the excited polarization for specific spectral peaks, as visualized in Fig. 9, the deposited power into the nanostructure as a result of its interaction with the field can be computed, shown in Fig. 10. To account for the temperature T changes, brought about by the optical

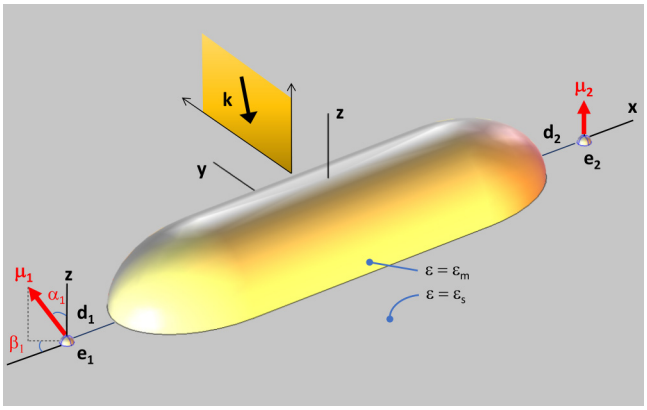

FIG. 6. An example of a basic substrate-bound nanoparticle for integrated plasmonics. Shown is a nanorod-type metallic particle with a dielectric function of ε_m placed on a substrate with a dielectric function ε_s. A number of quantum emitters e_i, $i = 1, 2$ with dipole moments $\bar{\mu}_i$, $i = 1, 2$ may be brought into interaction with the particle. The angles α_1 and β_1 depict a possible orientation of the first emitter. Other types of nanoparticles, substrates, emitters, and their configurational relations can be similarly envisioned. A field with momentum $\bar{k}$, here arbitrarily shown in a plane of incidence perpendicular to the x axis, interacts with the nanoparticle and the emitters. The system may be assumed thermodynamically open.

losses, we may solve the heat diffusion equation. Neglecting heat flux by radiation and convection (nanometer-scale surface area), and with zero velocity vector for the subdomain translational motion, we solve $T(\boldsymbol{r}, t)$: $-\nabla \cdot k\nabla T + \rho C T_t = \mathcal{S}(\lambda)$, where ρ, C, and k are, respectively, the density, heat capacity, and thermal conductivity of gold or quartz, while $\mathcal{S}$ is the wavelength-dependent λ source term. In general, k is a symmetric positive-definite second-order tensor. Thus, the ensuing thermoelastic effect generates a source term $-\boldsymbol{\alpha} T : d\boldsymbol{\sigma}/dt$, where $\boldsymbol{\alpha}$ is the thermal expansion coefficient, d/dt is the time derivative operator in the material frame, and $\boldsymbol{\sigma}$ is the stress distribution. The temperature changes yields an effective mechanical force. By solving the equation of motion, we thus compute the mechanical eigenmodes of the nanoparticle. By solving the heat diffusion equation with the source term provided by the optical losses, as can be seen in Fig. 11, the time evolution is seen to be sufficiently fast that, as far as energy diffusion is concerned, one may assume that the deposited power is instantaneous and uniform. From the solution of the diffusion equation, we can therefore obtain the energy transport from the nanoparticle into the surrounding domain via radiation and conduction but neglecting convective transport. Inclusion of the dielectric substrate will not only red shift plasmon energies but also facilitate a new transport channel for the dissipated heat energy.

We also note that when the radius of the structure is smaller than the electron mean free path, the losses are larger [43]. Classical computational calculation of the nonradiative losses (leading to very effective localized heating) can be informative. The generated heat makes the plasmonic nanostructure a very effective heat source for applications such as killing cancer cells and microfluidic actuation. Other than presenting a quantitative assessment of the nonradiative losses, the effect does not play a significant role for the objectives of

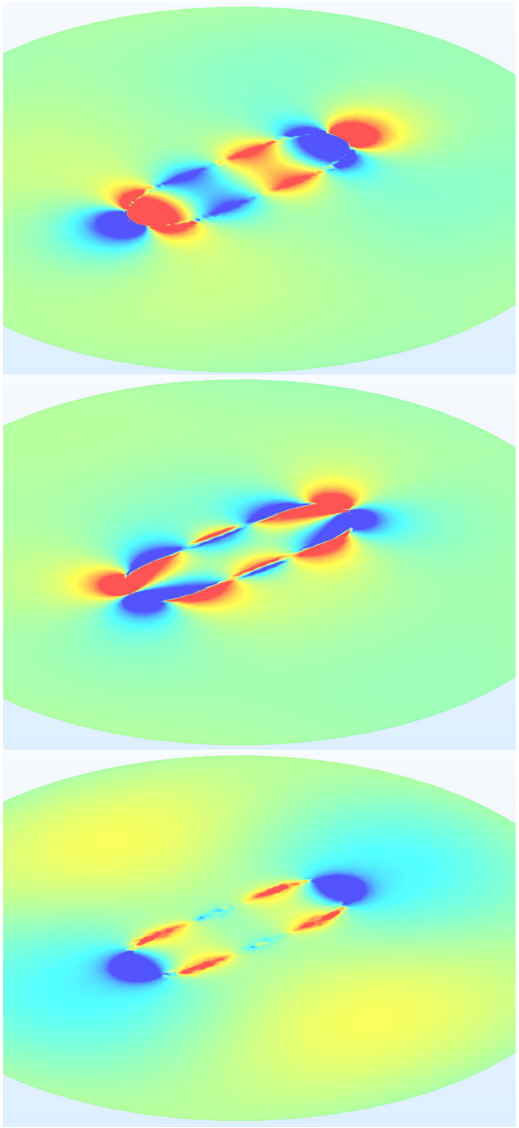

FIG. 7. Field component distribution E_x (top), E_y (middle), and E_z (bottom) engendered in the nanoparticle by two dipoles symmetrically placed along the long axis of the nanoparticle. The dipoles emit at a wavelength of 535 nm with their moments parallel to the z axis.

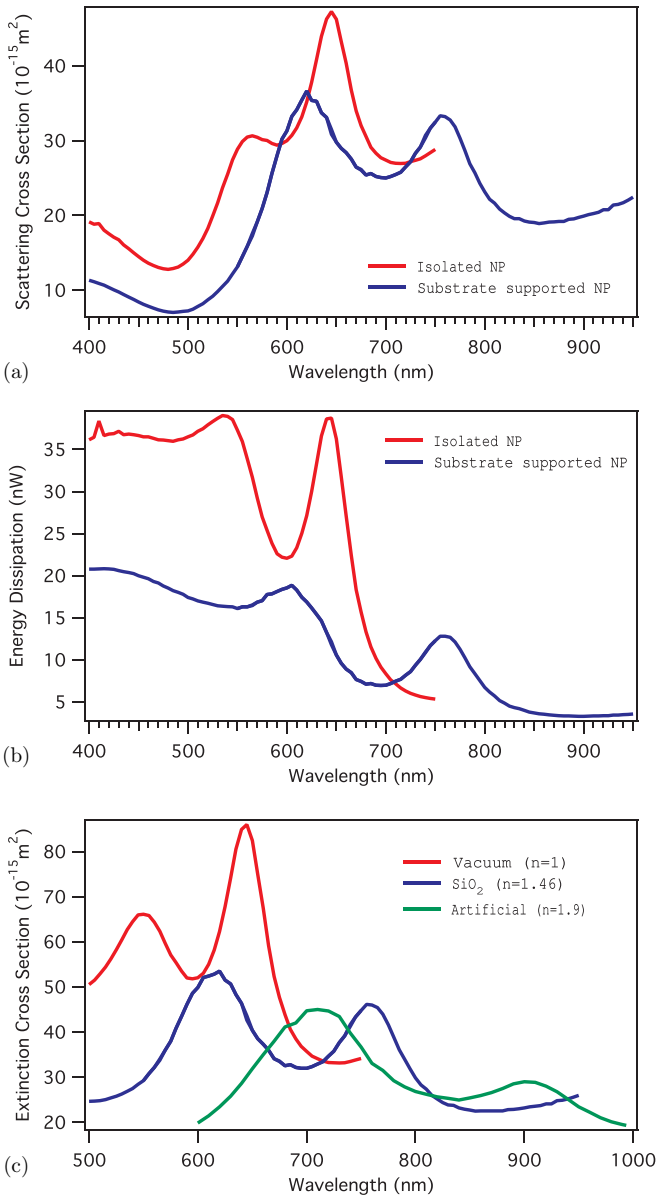

FIG. 8. The spectral properties of the nanoparticle shown in Fig. 6. For a 400-nm-long gold nanoparticle with prolate spheroidal end curvature (long axis 77 nm, short axis 50 nm), the scattering of photons exhibit two main peaks (≈535 nm and 642 nm) corresponding to excitation of the longitudinal and cross-sectional excitations. In addition to the substrate-induced plasmon damping, the two primary bands are observed to undergo a red shift and broadening as shown for the scattering cross section (a) and for the energy dissipation (b). The worsening of the spectral quality due to the substrate is shown (c) for the fused silica substrate as well an artificial substrate with higher index n.

the present work (unless one attempts plasmon sensing or surface-enhanced *Raman* spectroscopy and imaging [44]). Indeed, due to the difficulties associated with calculation of the nonradiative losses, many reported works have simply neglected the photothermal effect. However, the effect is not only significant but must indeed be included in the calculations for proper assessment of for example Raman cross-section calculations of the surface enhancement. We introduced the term "thermoplasmonics" to emphasize the photothermal nature and processes associated with plasmon resonances

APPENDIX B: RETARDED DISPERSION RELATIONS

Cylindrical coordinates is given by

$$x = b\,\rho\cos\varphi, \quad y = b\,\rho\sin\varphi, \quad z = b\,z, \tag{B1}$$

where $\rho \in [0,\infty)$, $\varphi \in [-\pi,\pi]$, and $z \in (-\infty,\infty)$ with scale factors $h_\rho = h_z = b$ and $h_\varphi = b\rho$, and b as the scaling constant. The cylinder of revolution is the surface generated by the revolution of a line parallel to an axis, around this axis, here the z axis. Therefore, the resulting surface has azimuthal symmetry with respect to the z axis. A cylinder in the cylindrical coordinator could be obtained by fixing the coordinate component ρ as the radius of the cylinder, i.e., $\rho = \rho_0$.

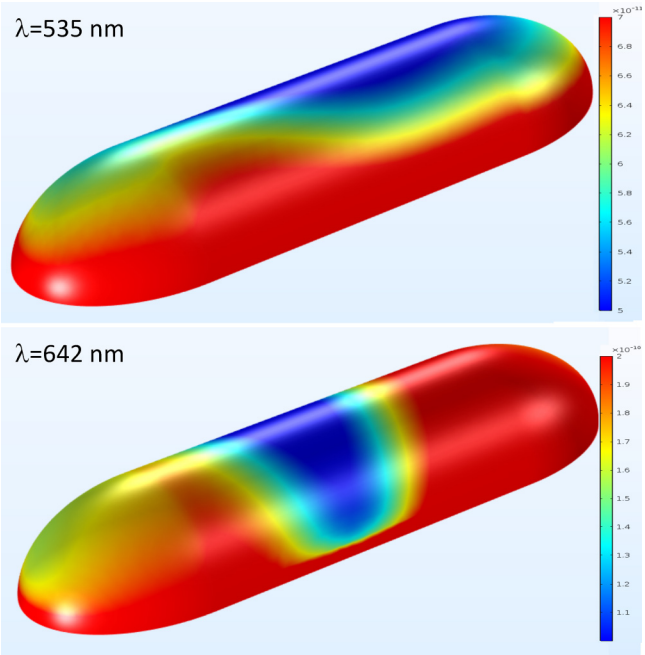

FIG. 9. Polarization distribution of the nanoparticle at the spectral peaks of the scattering cross section for an excitation field of a polarization that provides both axial and cross-sectional field components.

1. Helmholtz equation: Time-dependent dispersion relations

The Helmholtz equation in cylindrical coordinate has the closed from $\nabla^2\mathbf{E} + h^2\mathbf{E} = 0$, with ∇^2 denoting the Laplace operator, and is given by

$$\frac{1}{\rho}\frac{\partial}{\partial\rho}\left(\rho\frac{\partial\mathbf{E}}{\partial\rho}\right) + \frac{1}{\rho^2}\frac{\partial^2\mathbf{E}}{\partial\varphi^2} + \frac{\partial^2\mathbf{E}}{\partial z^2} + h^2\,\mathbf{E} = 0. \tag{B2}$$

The goal is to find the complex amplitude of the secondary field E satisfying the Helmholtz equation given above. The only possible set of solutions after considering the separation

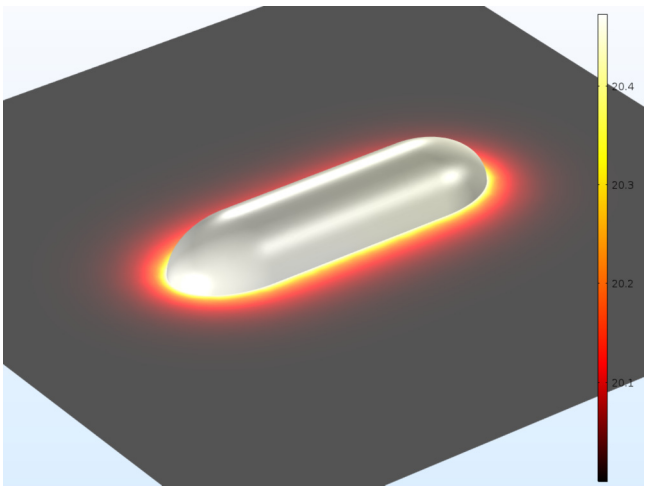

FIG. 10. Computed nanoparticle plasmon-induced heat generation for a gold nanorod on a quartz substrate.

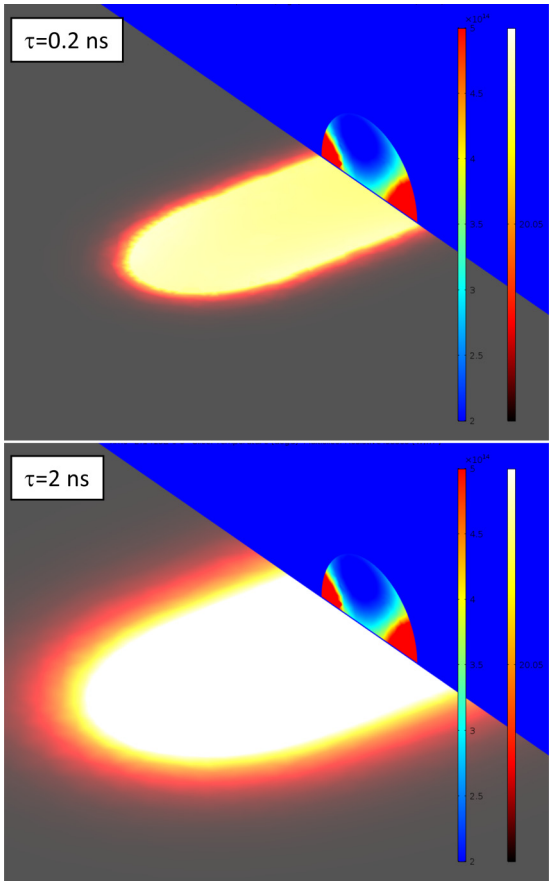

FIG. 11. Temperature distribution at $t = 0.2$ ns (top) and $t = 2$ ns (bottom) in the substrate plane due to energy losses in the nanoparticle. The energy loss density is visualized for an interacting field at a wavelength of 642 nm, corresponding to the plasmon excitation along the long axis of the nanoparticle.

of variables $\mathbf{E} = R(\rho)\,\Phi(\varphi)\,Z(z)$ is

$$\begin{aligned}\rho\,\frac{d}{d\rho}\left(\rho\frac{dR(\rho)}{d\rho}\right) + \left[\kappa^2\,\rho^2 - m^2\right]R(\rho) = 0,\\ \frac{d^2\Phi(\varphi)}{d\varphi^2} + m^2\Phi(\varphi) = 0,\\ \frac{d^2Z(z)}{dz^2} + k_z^2 Z(z) = 0,\end{aligned} \tag{B3}$$

where κ, m, and k are constants of x, y, and z with κ and k satisfying

$$\kappa^2 + k_z^2 = h^2. \tag{B4}$$

The final solution for a given set of κ, k_z, and m is given by

$$E_{\kappa km} = B_m(\kappa\,\rho)\,f(m\varphi)\,g(k_z z), \tag{B5}$$

where $B_m(\kappa\,\rho)$ is the combination of Bessel functions. Depending on the boundary conditions, it may be chosen among $J_m(\cdot)$ and $Y_m(\cdot)$, Bessel function of first and second kind, respectively, or $I_m(\cdot)$ and $K_m(\cdot)$, the modified Bessel function of first and second kind, respectively. The Hankel functions may be replaced by $J_m(\cdot)$ and $Y_m(\cdot)$, Bessel functions of the first and second kind, as an alternative representation

[45]. Lastly, the choice of modified Bessel functions for inside and outside of the solid cylinder lies in the asymptotic behaviors of these functions. $I_m(|k|\rho) \to \infty$ when $\rho \to \infty$ while $K_m(|k|\rho) \to \infty$ when $\rho \to 0$ [45].

In Eq. (B2), we may make the substitution

$$h^2 = \varepsilon \frac{\omega^2}{c^2}, \tag{B6}$$

as the corresponding total momentum, where ω is the angular frequency of the excitation and c denotes the so-called speed of light. We may define a solid cylinder as a surface of revolution by fixing $\rho = \rho_0$, and the position vector as $\mathbf{r} = (\rho, \varphi, z)$. One may impose the Dirichlet boundary condition (which specifies the value of the function on a surface, i.e., $\mathbf{E}_\mathrm{i} = \mathbf{E}_\mathrm{o}$ when $\rho = \rho_0$) as well as Neumann boundary condition which specifies the normal derivative of the function on a surface, as

$$\varepsilon_\mathrm{i}(\omega)\, \nabla \mathbf{E}_\mathrm{i} \cdot \tilde{\mathbf{n}}|_{\rho=\rho_0} = \varepsilon_\mathrm{o}(\omega)\, \nabla \mathbf{E}_\mathrm{o} \cdot \tilde{\mathbf{n}}|_{\rho=\rho_0}. \tag{B7}$$

2. Retarded dispersion relations

The interaction of the radiation field with matter, described as a scattering process, may exhibit strong spectral variation depending upon the geometric and material properties. Therefore, prior to quantization of the cylindrical surface waves to obtain the surface plasmon states, we consider electromagnetic normal modes of the solid domain as a starting point. With reference to Appendix B, solving the Helmholtz equation for points $\mathbf{r} = (\rho, \varphi, z)$ in a domain partitioned by an infinite cylinder of radius $\rho = \rho_0$, the solution set of eigenfunctions for the triple (κ, k_z, m) is given by

$$E_{\kappa k_z m} = B_m(\kappa\rho)\, f(m\varphi)\, g(k_z z),$$

where $B_m(\kappa\rho)$ is the combination of Bessel functions, as

$$B_m(\kappa\rho) \sim J_m(\kappa\rho)\, Y_m(\kappa\rho)\, I_m(\kappa\rho)\, K_m(\kappa\rho),$$

where $J_m(\cdot)$ and $Y_m(\cdot)$ denote the Bessel function of the first and second kind, respectively, and where $I_m(\cdot)$ and $K_m(\cdot)$ denote the modified Bessel functions of the first and second kind, respectively. The Bessel functions of the first and second kind, $J_m(\cdot)$ and $Y_m(\cdot)$, may also be replaced by the Hankel functions, $H_m^{(1)}(\kappa\rho)$, $H_m^{(2)}(\kappa\rho)$, also known as the Bessel functions of the third kind, as an alternative representation [45].

The choice of Bessel functions depends on two factors: (1) the radiative or nonradiative regime being considered and (2) the asymptotic behavior of the modified Bessel functions. More specifically, Bessel functions of the first and second kinds, $J_m(\cdot)$ and $Y_m(\cdot)$, are associated with the radiative regime, whereas modified Bessel functions of the first and second kinds, $I_m(\cdot)$ and $K_m(\cdot)$, represent the nonradiative regime. The radiative regime requires [as will be seen from Eq. (B9) and the light line in Fig. 2], up to some constant, $B_m(\kappa\rho) = J_m(\kappa\rho)\, H_m^{(1)}(\kappa\rho)$, while for the nonradiative regime $B_m(\kappa\rho) = I_m(\kappa\rho)\, K_m(\kappa\rho)$. In the interior versus exterior of the cylinder, we note $I_m(\kappa\rho) \to \infty$ when $\rho \to \infty$ while $K_m(\kappa\rho) \to \infty$ when $\rho \to 0$ [45].

To simplify the equations, after partitioning the space with the Heaviside function Θ, with the half-maximum convention, $\Theta(0) = 1/2$, we introduce $\theta_m^<(\kappa, \rho)$ and $\theta_m^>(\kappa, \rho)$ as given in Eqs. (2) and (3). In the nonradiative regime, the solutions may be obtained for the z component of the electric field as

$$E_z(\mathbf{r}, t) = \sum_{m=-\infty}^{\infty} \mathscr{C}_m(t) e^{i(k_z z + m\varphi - \omega t)} \times [\theta_m^<(\kappa_\mathrm{i}, \rho) + \theta_m^>(\kappa_\mathrm{o}, \rho)], \tag{B8}$$

where $\mathscr{C}_m(t)$ is the complex quasistatic mode amplitude at time t, with $m \in \mathbb{Z}$, counting the azimuthal modes. Here, k_z is the magnitude of the wave vector along the cylinder axis, κ is the transverse momentum, indexed to indicate the interior and exterior domains (κ_i and κ_o) of the solid, and ω is the field frequency. Alternatively, one may rewrite Eq. (1) using the Euler relation for the azimuthal solutions with the consideration that now $m \in \mathbb{N} + \{0\}$, and for a fixed value of m, there are two different sets of solutions depending on the branches in $\sin(\cdot)$ or $\cos(\cdot)$. The remaining field components can be written as

$$E_\varphi(\mathbf{r}, t) = \sum_{m=-\infty}^{\infty} \left[-\frac{hm}{\kappa^2 \rho} \mathscr{D}_m(t) I_m(\kappa\rho) + \frac{i\omega}{\kappa} \mathscr{E}_m(t) K_m'(\kappa\rho) \right]$$

and

$$E_\rho(\mathbf{r}, t) = \sum_{m=-\infty}^{\infty} \left[-\frac{m\omega}{\kappa^2 \rho} \mathscr{F}_m(t) I_m(\kappa\,\rho) + \frac{ih}{\kappa} \mathscr{G}_m(t) K_m'(\kappa\rho) \right].$$

Since $\kappa^2 + k_z^2 = h^2$, we may use Eqs. (B4) and (B6) to write

$$\begin{aligned} \kappa_\mathrm{i}^2 &= k_z^2 - h_\mathrm{i}^2 = k_z^2 - \omega^2 \varepsilon_\mathrm{i}(\omega)/c^2, \\ \kappa_\mathrm{o}^2 &= k_z^2 - h_\mathrm{o}^2 = k_z^2 - \omega^2 \varepsilon_\mathrm{o}(\omega)/c^2, \end{aligned} \tag{B9}$$

where ε_i and ε_o denote the values of the dielectric functions at frequency ω for the interior and exterior domains, respectively. Imposing Dirichlet and Neumann boundary conditions [see Eq. (B7)] results in

$$\begin{aligned} &(c\rho_0 \kappa_\mathrm{i} \kappa_\mathrm{o})^2 \left(\kappa_\mathrm{o}^2\, \varepsilon_\mathrm{i} \mathcal{I}_m - \kappa_\mathrm{i}^2\, \varepsilon_\mathrm{o} \mathcal{K}_m\right)\left(\kappa_\mathrm{o}^2\, \mathcal{I}_m - \kappa_\mathrm{i}^2\, \mathcal{K}_m\right) \\ &\quad - [m\omega k_z (\varepsilon_\mathrm{o} - \varepsilon_\mathrm{i})]^2 = 0, \end{aligned} \tag{B10}$$

where $\mathcal{I}_m$ and $\mathcal{K}_m$ are given in Eqs. (5) and (6), for $m = 0, 1, 2, \ldots$ (also see Ref. [20]). We later show that Eq. (B10) reduces to the quasistatic dispersion relations when $c \to \infty$. Considering the dielectric properties of the involved media $\varepsilon_\mathrm{i}/\varepsilon_\mathrm{o}$, we may assume $\varepsilon_\mathrm{o} = 1$ and $\varepsilon_\mathrm{i}(\omega) = \varepsilon(\omega)$, that is, a vacuum-bounded solid cylinder with a local frequency-dependent dielectric function. Solving Eq. (B10) explicitly for ε, one may obtain

$$\varepsilon(\omega) = \frac{\kappa_\mathrm{i}^3\, \kappa_\mathrm{o}^3\, \mathcal{I}_m\, \mathcal{K}_m - \kappa_\mathrm{i}^4\, \kappa_\mathrm{o}^2\, \mathcal{K}_m^2 + (m\omega_p k_z/\rho_0)^2}{\kappa_\mathrm{i}^2\, \kappa_\mathrm{o}^4\, \mathcal{I}_m^2 - \kappa_\mathrm{i}^3\, \kappa_\mathrm{o}^3\, \mathcal{I}_m\, \mathcal{K}_m + (m\omega_p k_z/\rho_0)^2}. \tag{B11}$$

The energies of the first few plasmon modes m in Fig. 2 correspond to set of pairs (k_z, ω) for which Eq. (B10) is zero, that is, for each m, the roots (k_z, ω) of the implicit function Eq. (B10) are found and enhanced by interpolation. The results agree well with reported cylindrical surface modes [8,21]. The solutions on the right-hand side of the light line $\omega = c\, k_z$ correspond to the nonradiative regime (whereas the radiative regime solutions will appear on the left-hand side, not displayed).

APPENDIX C: QUASISTATIC DISPERSION RELATION

The quasistatic plasmon dispersion relations may be obtained from Eq. (B10) when $c \to \infty$. Alternatively, they may also be obtained directly from the scalar potentials satisfying the Laplace equation. In Appendix C, we have shown that our solution Eq. (B10) agrees well with the special case of that of a multilayered cylinder [8]. In the quasistatic limit, $c \to \infty$, Eq. (B10) reduces to

$$\left[\kappa_{\rm o}\,\varepsilon(\omega)\,\frac{I_m'(\kappa_{\rm i}\,\rho_0)}{I_m(\kappa_{\rm i}\,\rho_0)} - \kappa_{\rm i}\,\frac{K_m'(\kappa_{\rm o}\,\rho_0)}{K_m(\kappa_{\rm o}\,\rho_0)}\right] \times \left[\kappa_o\,\frac{I_m'(\kappa_i\,\rho_0)}{I_m(\kappa_i\,\rho_0)} - \kappa_i\,\frac{K_m'(\kappa_o\,\rho_0)}{K_m(\kappa_o\,\rho_0)}\right] = 0. \tag{C1}$$

Observing Eqs. (B9) in this limit, we have $|\kappa_{\rm i}| = |\kappa_{\rm o}| = |k_z| = \kappa$, and since the Wronskian of the modified Bessel functions prevents the second bracket in Eq. (C1) from being zero, we obtain, for a Drude metal of plasma frequency ω_p, the energy of a surface plasmon mode (m, κ)

$$\begin{aligned}\hbar\omega_{m\kappa} &= \hbar\omega_p\sqrt{\frac{I_m'(|\kappa|\,\rho_0)\,K_m(|\kappa|\,\rho_0)}{\mathcal{W}\{I_m(|\kappa|\,\rho_0),\,K_m(|\kappa|\,\rho_0)\}}}\\ &= \hbar\omega_p\sqrt{|\kappa|\,\rho_0\,I_m'(|\kappa|\,\rho_0)\,K_m(|\kappa|\,\rho_0)},\end{aligned}$$

where the last expression is obtained from the fact that the Wronskian satisfies the identity [46,47] $\mathcal{W}\{I_m(z), K_m(z)\} = z^{-1}$, which agrees with the cylindrical limit frequency given in Eq. 3.10 in Ref. [48]. The results are shown in Fig. 3. In greater detail, given explicitly in [8], the non-quasi-static solution for frequencies are expressed as the following determinant:

$$\begin{vmatrix}\tau_{m-1} & \varphi_m\\ \zeta_m & \nu_{m-1}\end{vmatrix} = 0, \tag{C2}$$

whose solutions for a double-nanowire system are given in Ref. [21] as

$$\kappa_i^2\,\kappa_o^2\left[\kappa_o\,\varepsilon_i\,\frac{I_m'(\kappa_i\,\rho)}{I_m(\kappa_i\,\rho)} - \kappa_i\,\varepsilon_o\,\frac{K_m'(\kappa_o\,\rho)}{K_m(\kappa_o\,\rho)}\right] \times \left[\kappa_o\,\frac{I_m'(\kappa_i\,\rho)}{I_m(\kappa_i\,\rho)} - \kappa_i\,\frac{K_m'(\kappa_o\,\rho)}{K_m(\kappa_o\,\rho)}\right] - \frac{m^2\,k^2}{\rho^2}\,(\varepsilon_o - \varepsilon_i)\frac{\omega^2}{c^2} = 0. \tag{C3}$$

On the one hand, without loss of generality, one may assume the geometry is placed in a void with $\varepsilon_o = 1$, $\varepsilon_i = \varepsilon$, and $\kappa_i = \kappa_o = \kappa$. Hence,

$$\kappa^4\left[\kappa\,\varepsilon(\omega)\,\frac{I_m'(\kappa\,\rho)}{I_m(\kappa\,\rho)} - \kappa\,\frac{K_m'(\kappa\,\rho)}{K_m(\kappa\,\rho)}\right] \times \left[\kappa\,\frac{I_m'(\kappa\,\rho)}{I_m(\kappa\,\rho)} - \kappa\,\frac{K_m'(\kappa\,\rho)}{K_m(\kappa\,\rho)}\right] - \frac{m^2\,k^2}{\rho^2}\,[1-\varepsilon(\omega)]\frac{\omega^2}{c^2} = 0. \tag{C4}$$

Using the relation $\omega_p^2/\omega^2 = 1 - \varepsilon$, we have

$$\kappa^4\left[\kappa\,\varepsilon(\omega)\,\frac{I_m'(\kappa\,\rho)}{I_m(\kappa\,\rho)} - \kappa\,\frac{K_m'(\kappa\,\rho)}{K_m(\kappa\,\rho)}\right] \times \left[\kappa\,\frac{I_m'(\kappa\,\rho)}{I_m(\kappa\,\rho)} - \kappa\,\frac{K_m'(\kappa\,\rho)}{K_m(\kappa\,\rho)}\right] - \frac{m^2\,k_z^2}{\rho^2}\,[1-\varepsilon(\omega)]\frac{\omega^2}{c^2} = 0. \tag{C5}$$

Therefore,

$$\left[\left(1-\omega_p^2/\omega^2\right)\frac{I_m'(\kappa\,\rho)}{I_m(\kappa\,\rho)} - \frac{K_m'(\kappa\,\rho)}{K_m(\kappa\,\rho)}\right]\left[\frac{I_m'(\kappa\,\rho)}{I_m(\kappa\,\rho)} - \frac{K_m'(\kappa\,\rho)}{K_m(\kappa\,\rho)}\right] - \frac{m^2\,k^2}{\kappa^6\,\rho^2}\,\frac{\omega_p^2}{c^2} = 0. \tag{C6}$$

Using notations introduced in Eqs. (5) and (6), after some algebra, one may find

$$\frac{\omega_p^2}{\omega_m^2} = \frac{(\mathcal{I}_m - \mathcal{K}_m)^2 - \frac{m^2\,k^2\,\omega_p^2}{\kappa^6\,\rho^2\,c^2}}{\mathcal{I}_m^2 - \mathcal{I}_m\,\mathcal{K}_m}, \tag{C7}$$

which indicates the exact frequency for the cylinder.

On the other hand, in a quasistatic limit, if one lets $c \to \infty$, the above equation simplifies to

$$\left[\kappa_o\,\varepsilon_i\,\frac{I_m'(\kappa_i\,\rho)}{I_m(\kappa_i\,\rho)} - \kappa_i\,\varepsilon_o\,\frac{K_m'(\kappa_o\,\rho)}{K_m(\kappa_o\,\rho)}\right] \times \left[\kappa_o\,\frac{I_m'(\kappa_i\,\rho)}{I_m(\kappa_i\,\rho)} - \kappa_i\,\frac{K_m'(\kappa_o\,\rho)}{K_m(\kappa_o\,\rho)}\right] = 0, \tag{C8}$$

which implies at least one of the brackets to be zero. The second bracket is never zero considering the Wronskian for modified Bessel functions (see below). Hence,

$$\kappa\,\varepsilon\,\frac{I_m'(\kappa\,\rho)}{I_m(\kappa\,\rho)} - \kappa\,\frac{K_m'(\kappa\,\rho)}{K_m(\kappa\,\rho)} = 0 \tag{C9}$$

and

$$\varepsilon = \frac{I_m(\kappa\,\rho)}{I_m'(\kappa\,\rho)}\,\frac{K_m'(\kappa\,\rho)}{K_m(\kappa\,\rho)}. \tag{C10}$$

This relation could also be obtained by letting $c \to \infty$ as in Eq. (B10). Using the relation $\omega_p^2/\omega^2 = 1 - \varepsilon$, we may write

$$\begin{aligned}\frac{\omega_p^2}{\omega_m^2} &= 1 - \frac{I_m(\kappa\,\rho)}{I_m'(\kappa\,\rho)}\,\frac{K_m'(\kappa\,\rho)}{K_m(\kappa\,\rho)}\\ &= \frac{I_m'(\kappa\,\rho)\,K_m(\kappa\,\rho) - I_m(\kappa\,\rho)\,K_m'(\kappa\,\rho)}{I_m'(\kappa\,\rho)\,K_m(\kappa\,\rho)}\\ &= \frac{\mathcal{W}\{I_m(\kappa\,\rho), K_m(\kappa\,\rho)\}}{I_m'(\kappa\,\rho)\,K_m(\kappa\,\rho)},\end{aligned} \tag{C11}$$

where $\mathcal{W}\{I_m(\kappa\,\rho), K_m(\kappa\,\rho)\}$ denotes the so-called Wronskian. Using Ref. [46]

$$\mathcal{W}\{I_m(z), K_m(z)\} = \frac{1}{z},$$

one may write

$$\frac{\omega_p^2}{\omega_m^2} = \frac{1}{\kappa\,\rho\,I_m'(\kappa\,\rho)\,K_m(\kappa\,\rho)}, \tag{C12}$$

which is the same as the cylindrical limit frequency given in Eq. (3.10) in Ref. [48]. In the following section, we obtain this relation independently by considering the retarded potential and solving Laplace equation on the boundary of a solid cylinder.

APPENDIX D: QUASISTATIC LIMIT

Laplace equation in cylindrical coordinate (ρ, φ, z) is given by

$$\nabla^2\Phi = \frac{1}{b^2}\left\{\frac{1}{\rho}\frac{\partial}{\partial\rho}\left(\rho\frac{\partial}{\partial\rho}\right) + \frac{1}{\rho^2}\frac{\partial^2}{\partial\varphi^2} + \frac{\partial^2}{\partial z^2}\right\}\Phi. \quad \text{(D1)}$$

Letting $\Phi(\rho, \varphi, z) = R(\rho)\Theta(\varphi)Z(z)$ gives

$$\begin{aligned} \frac{d^2Z}{dz^2} - k^2Z &= 0, \\ \frac{d^2\Theta}{d\varphi^2} + m^2\Theta &= 0, \\ \frac{d^2R}{d\rho^2} + \frac{1}{\rho}\frac{dR}{d\rho} + \left(k^2 - \frac{m^2}{\rho^2}\right)R &= 0, \end{aligned} \quad \text{(D2)}$$

and replacing k with ik gives

$$\begin{aligned} \frac{d^2Z}{dz^2} + k^2Z &= 0, \\ \frac{d^2\Theta}{d\varphi^2} + m^2\Theta &= 0, \\ \frac{d^2R}{d\rho^2} + \frac{1}{\rho}\frac{dR}{d\rho} - \left(k^2 + \frac{m^2}{\rho^2}\right)R &= 0. \end{aligned} \quad \text{(D3)}$$

Considering the Dirichlet and Neumann boundary conditions, one may define

$$\Phi(\mathbf{r}, t) = \Theta(\rho_0 - \rho)\Phi_{\rm i}(\mathbf{r}, t) + \Theta(\rho - \rho_0)\Phi_{\rm o}(\mathbf{r}, t), \quad \text{(D4)}$$

where

$$\begin{aligned} \Phi_{\rm i}(\mathbf{r}, t) = \sum_{m=-\infty}^{\infty} e^{im\varphi} \int_{-\infty}^{\infty} & C_{mk}(t) I_m(|k|\rho) K_m(|k|\rho_0) \\ & \times e^{ikz}\, dk, \quad \rho \leqslant \rho_0, \end{aligned} \quad \text{(D5)}$$

and

$$\begin{aligned} \Phi_{\rm o}(\mathbf{r}, t) = \sum_{m=-\infty}^{\infty} e^{im\varphi} \int_{-\infty}^{\infty} & C_{mk}(t) I_m(|k|\rho_0) K_m(|k|\rho) \\ & \times e^{ikz}\, dk, \quad \rho_0 \leqslant \rho. \end{aligned} \quad \text{(D6)}$$

Hence, the Laplacian becomes

$$\begin{aligned} \nabla^2\Phi(\mathbf{r}, t) = \frac{\delta(\rho - \rho_0)}{b^2}\left(\frac{\partial\Phi_{\rm o}}{\partial\rho} - \frac{\partial\Phi_{\rm i}}{\partial\rho}\right) \\ + \Theta(\rho_0 - \rho)\nabla^2\Phi_{\rm i}(\mathbf{r}, t) \\ + \Theta(\rho - \rho_0)\nabla^2\Phi_{\rm o}(\mathbf{r}, t). \end{aligned} \quad \text{(D7)}$$

Since we are only interested on the surface and since the Laplacian vanishes inside and outside, then

$$\nabla^2\Phi(\mathbf{r}, t) = \frac{\delta(\rho - \rho_0)}{b^2}\left(\frac{\partial\Phi_{\rm o}}{\partial\rho} - \frac{\partial\Phi_{\rm i}}{\partial\rho}\right). \quad \text{(D8)}$$

Using (7), we have

$$\begin{aligned} \frac{\partial\Phi_{\rm o}}{\partial\rho} - \frac{\partial\Phi_{\rm i}}{\partial\rho} &= \sum_{m=-\infty}^{\infty} e^{im\varphi} \int_{-\infty}^{\infty} |k|\, C_{mk}(t) \\ &\quad \times \mathcal{W}\{I_m(|k|\rho), K_m(|k|\rho)\} e^{ikz}\, dk \\ &= -\sum_{m=-\infty}^{\infty} e^{im\varphi} \int_{-\infty}^{\infty} \rho^{-1}\, C_{mk}(t) e^{ikz}\, dk, \end{aligned} \quad \text{(D9)}$$

and using Wronskian identity gives

$$\mathcal{W}\{I_m(|k|\rho), K_m(|k|\rho)\} = -\frac{1}{|k|\rho}. \quad \text{(D10)}$$

Using relation $h_\rho\nabla^2\Phi = -4\pi\delta(\rho - \rho_0)\sigma$, we get

$$\sigma = \frac{1}{4\pi b\rho_0} \sum_{m=-\infty}^{\infty} e^{im\varphi} \int_{-\infty}^{\infty} C_{mk}(t) e^{ikz}\, dk, \quad \text{(D11)}$$

so therefore

$$\ddot{\sigma} = \frac{1}{4\pi b\rho_0} \sum_{m=-\infty}^{\infty} e^{im\varphi} \int_{-\infty}^{\infty} \ddot{C}_{mk}(t) e^{ikz}\, dk. \quad \text{(D12)}$$

On the other hand,

$$\begin{aligned} \ddot{\sigma} = -\frac{\omega_p^2}{4\pi b} \sum_{m=-\infty}^{\infty} e^{im\varphi} \int_{-\infty}^{\infty} & |k| C_{mk}(t) I'_m(|k|\rho_0) \\ & \times K_m(|k|\rho_0) e^{ikz}\, dk. \end{aligned} \quad \text{(D13)}$$

Putting (D12) and (D13) equal and using the orthogonality in m and φ and also q and z, we get equation of motion and frequency as shown in Eq. (8).

APPENDIX E: TOTAL ENERGY OF CYLINDRICAL CHARGES

Potential energy is given by

$$V = \frac{1}{2}\int_{-\pi}^{\pi}\int_{-\infty}^{\infty} \sigma\, \Phi_{\rm i}|_{\rho=\rho_0} h_z h_\varphi\, dz d\varphi,$$

and then

$$\begin{aligned} V = \frac{b\rho_0\omega_p^2}{8\pi} \sum_{m,m'} \int_{-\pi}^{\pi} e^{i(m-m')\varphi}\, d\varphi \\ \times \int_{-\infty}^{\infty} \left\{ \int_{-\infty}^{\infty}\int_{-\infty}^{\infty} |k| \frac{C_{mk}(t)}{\omega_{mk}^2} \overline{C_{m'k'}}(t) \right. \\ \times I'_m(|k|\rho_0) I_{m'}(|k'|\rho_0) K_m(|k|\rho_0) K_{m'}(|k'|\rho_0) \\ \left. \times e^{i(k-k')z}\, dk\, dk' \right\} dz, \end{aligned} \quad \text{(E1)}$$

as we replaced real-valued potential with its complex conjugate. Considering the orthogonality relations

$$\int_{-\pi}^{\pi} e^{i(m-m')\varphi} d\varphi = 2\pi\ \delta_{mm'}, \quad \text{(E2)}$$

and

$$\int_{-\infty}^{\infty} e^{i(k-k')z}\, dz = 2\pi\delta(k - k'), \quad \text{(E3)}$$

where $\delta_{mm'}$ denotes the Kronecker delta functions and $\delta(k-k')$ is the Dirac delta function, it follows that (E1) can be written as

$$V = \frac{\pi b \rho_0 \omega_p^2}{2} \sum_{m=-\infty}^{\infty} \int_{-\infty}^{\infty} \frac{|k|}{\omega_{mk}^2} \left|C_{mk}(t)\right|^2 \times I_m(|k|\rho_0) I'_m(|k|\rho_0) [K_m(|k|\rho_0)]^2 \, dk, \tag{E4}$$

or, using (8),

$$V = \frac{\pi b}{2} \sum_{m=-\infty}^{\infty} \int_{-\infty}^{\infty} |C_{mk}(t)|^2 I_m(|k|\rho_0) K_m(|k|\rho_0) \, dk. \tag{E5}$$

Similar calculations give kinetic energy as

$$T = \frac{\pi b \rho_0 \omega_p^2}{2} \sum_{m=-\infty}^{\infty} \int_{-\infty}^{\infty} \frac{|k|}{\omega_{km}^4} |\dot{C}_{mk}(t)|^2 I_m(|k|\rho_0) I'_m(|k|\rho_0) \times [K_m(|k|\rho_0)]^2 \, dk. \tag{E6}$$

Following symmetry relations for modified Bessel functions [47], Eq. (5.7.10), page 110,

$$\begin{cases} I_m(z) = I_{-m}(z); & \text{for} \quad m \in \mathbb{Z}, \\ k_\nu(z) = k_{-\nu}(z); & \text{for} \quad \nu \in \mathbb{R}, \end{cases} \tag{E7}$$

where for integers $\nu = n$, $k_n(z) = \lim_{\nu \to n} k_\nu(z)$, then

$$\begin{aligned} k_n(z) &= \lim_{\nu \to n} k_\nu(z) \\ &= \lim_{-\nu \to n} k_{-\nu}(z) \overset{(E7)}{=} \lim_{-\nu \to n} k_\nu(z) \\ &\lim_{\nu \to -n} k_\nu(z) = k_{-n}(z), \end{aligned} \tag{E8}$$

and hence $k_n(z) = k_{-n}(z)$ for $n \in \mathbb{Z}$.

APPENDIX F: ON THE COMPLEX AMPLITUDES

Recalling the inside scalar potential relation as

$$\Phi_{\rm i}(\mathbf{r}, t) = \sum_{m=-\infty}^{\infty} e^{im\varphi} \int_{-\infty}^{\infty} C_{mk}(t) I_m(|k|\rho) K_m(|k|\rho_0) e^{ikz} \, dk, \tag{F1}$$

the conjugate of the potential is hence given by

$$\overline{\Phi_{\rm i}}(\mathbf{r}, t) = \sum_{m=-\infty}^{\infty} e^{-im\varphi} \int_{-\infty}^{\infty} \overline{C_{mk}}(t) I_m(|k|\rho) K_m(|k|\rho_0) \times e^{-ikz} \, dk, \tag{F2}$$

and by letting $m \to -m$ and $k \to -k$, we have

$$\overline{\Phi_{\rm i}}(\mathbf{r}, t) = \sum_{m=-\infty}^{\infty} e^{im\varphi} \int_{-\infty}^{\infty} \overline{C_{-m-k}}(t) I_{-m}(|k|\rho) \times K_{-m}(|k|\rho_0) e^{ikz} \, dk. \tag{F3}$$

Using symmetry relations for modified Bessel functions given in (E7) [47], we have

$$\overline{\Phi_{\rm i}}(\mathbf{r}, t) = \sum_{m=-\infty}^{\infty} e^{im\varphi} \int_{-\infty}^{\infty} \overline{C_{-m-k}}(t) I_m(|k|\rho) K_m(|k|\rho_0) e^{ikz} \, dk, \tag{F4}$$

and since potential is real valued, then $\Phi_{\rm i}(\mathbf{r}, t) = \overline{\Phi_{\rm i}}(\mathbf{r}, t)$, which implies

$$C_{mk}(t) = \overline{C_{-m-k}}(t) \tag{F5}$$

for all m and k. The complex coefficients $C_{mk}(t)$ could be written as

$$C_{mk}(t) = \frac{\gamma_{mk}}{\omega_{mk}} c_{mk}, \tag{F6}$$

where c_{mk} are some complex function (of time) proportional to $e^{-i\omega_{mk}t}$ in which symmetric (in m and k) coefficients γ_{mk} would be determined later. One could write

$$\begin{aligned} C_{mk}(t) &= \frac{1}{2}[C_{mk}(t) + C_{mk}(t)] \\ &\overset{(F5)}{=} \frac{1}{2}[C_{mk}(t) + \overline{C_{-m-k}}(t)] \\ &= \frac{\gamma_{mk}}{2\omega_{mk}}(c_{mk} + \overline{c_{-m-k}}) \\ &= \frac{\gamma_{mk}}{2\omega_{mk}}(c_{mk} + c^*_{-m-k}), \end{aligned} \tag{F7}$$

and note that according to (8), since $\omega_{mk} = \omega_{-m-k}$, we could factor it out. Its time derivative gives

$$\dot{C}_{mk}(t) = -i\gamma_{mk} \, c^*_{mk}; \tag{F8}$$

similarly,

$$\begin{aligned} \dot{C}_{mk}(t) &= \frac{1}{2}[\dot{C}_{mk}(t) + \dot{C}_{mk}(t)] \\ &= \frac{1}{2}\big[\dot{C}_{mk}(t) + \overline{\dot{C}_{-m-k}}(t)\big] \\ &\overset{(F8)}{=} \frac{\gamma_{mk}}{2}\big(-ic^*_{mk} + ic_{-m-k}\big) \\ &= \frac{i\gamma_{mk}}{2}(c_{mk} - c^*_{-m-k}). \end{aligned} \tag{F9}$$

[1] H. Yu, Y. Peng, Y. Yang, and Z. Y. Li, Plasmon-enhanced light–matter interactions and applications, npj Comput. Mater. **5**, 45 (2019).

[2] M. Salhi, A. Passian, and G. Siopsis, Toroidal nanotraps for cold polar molecules, Phys. Rev. A **92**, 033416 (2015).

[3] S. Keramati, A. Passian, V. Khullar, J. Beck, C. Uiterwaal, and H. Batelaan, Surface plasmon enhanced fast electron emission from metallised fibre optic nanotips, New J. Phys. **22**, 083069 (2020).

[4] A. V. Savin, E. A. Korznikova, and S. V. Dmitriev, Twistons in graphene nanoribbons on a substrate, Phys. Rev. B **102**, 245432 (2020).

[5] P. B. Allen, Nanocrystalline nanowires: 2. Phonons, Nano Lett. **7**, 11 (2007).

[6] A. Passian and N. Imam, Nanosystems, edge computing, and the next generation computing systems, Sensors **19**, 4048 (2019).

[7] D. Niu, M. Zerrad, A. Lereu, A. Moreau, J. Lumeau, J. A. Zapien, A. Passian, V. Aubry, and C. Amra, Excitation of Bloch Surface Waves in Zero-Admittance Multilayers for High-Sensitivity Sensor Applications, Phys. Rev. Applied **13**, 054064 (2020).

[8] J. Pritz and L. M. Woods, Surface plasmon polaritons in concentric cylindrical structures, Solid State Commun. **146**, 345 (2008).

[9] A. Passian, A. L. Lereu, E. T. Arakawa, A. Wig, T. Thundat, and T. L. Ferrell, Modulation of multiple photon energies by use of surface plasmons, Opt. Lett. **30**, 41 (2005).

[10] H. Barlow, Surface waves supported by cylindrical surfaces, IRE Trans. Antennas Propagation **7**, 147 (1959).

[11] H. M. Barlow and A. L. Cullen, Surface waves, Proc. IEE Part III **100**, 329 (1953).

[12] E. Dumitrescu and B. Lawrie, Antibunching dynamics of plasmonically mediated entanglement generation, Phys. Rev. A **96**, 053826 (2017).

[13] T. M. D. Alharbi, Y. Shingaya, K. Vimalanathan, T. Nakayama, and C. L. Raston, High yielding fabrication of magnetically responsive coiled single-walled carbon nanotube under flow, ACS Appl. Nano Mater. **2**, 5282 (2019).

[14] H. Iwase and T. Baba, Electromagnetic-field imbalance in surface plasmon polariton and its role in slow propagation and field-matter interaction, J. Opt. Soc. Am. B **36**, 1327 (2019).

[15] T. G. Pedersen, Plasmons and magnetoplasmon resonances in nanorings, Phys. Rev. B **103**, 085419 (2021).

[16] M. C. Ko, N. C. Kim, S. R. Ri, J. S. Ryom, S.l. Choe, I. H. Choe, Y. C. Kim, and G. I. An, Designable quantum beamsplitter using the two-level InGaAs quantum dot interacting with a Y-type plasmonic waveguide, Int. J. Mod. Phys. B **34**, 2050213 (2020).

[17] M. Bagherian, S. Kouchekian, I. Rothstein, and A. Passian, Quantization of surface charge density on hyperboloidal and paraboloidal domains with application to plasmon decay rate on nanoprobes, Phys. Rev. B **98**, 125413 (2018).

[18] M. Bagherian, A. Passian, S. Kouchekian, and G. Siopsis, Quantum Hamiltonian for the surface charge density on a ring torus and radiative decay of plasmons, Phys. Rev. B **102**, 085422 (2020).

[19] R. H. Ritchie, Plasma losses by fast electrons in thin films, Phys. Rev. **106**, 874 (1957).

[20] C. Ashley, Dispersion relations for non-radiative surface plasmons on cylinders, Surf. Sci. **41**, 615 (1974).

[21] S. Sun, H. T. Chen, W. J. Zheng, and G. Y. Guo, Dispersion relation, propagation length and mode conversion of surface plasmon polaritons in silver double-nanowire systems, Opt. Express **21**, 14591 (2013).

[22] A. L. Lereu, A. Passian, R. H. Farahi, N. F. Van Hulst, T. L. Ferrell, and T. Thundat, Thermoplasmonic shift and dispersion in thin metal films, J. Vacuum Sci. Technol. A **26**, 836 (2008).

[23] G. B. Folland, *Quantum Field Theory: A Tourist Guide for Mathematicians*, Vol. 149 (American Mathematical Society, Providence, Rhode Island, 2021).

[24] S. Raza, G. Toscano, A. P. Jauho, M. Wubs, and N. A. Mortensen, Unusual resonances in nanoplasmonic structures due to nonlocal response, Phys. Rev. B **84**, 121412 (2011).

[25] S. I. Bozhevolnyi and J. B. Khurgin, The case for quantum plasmonics, Nat. Photon. **11**, 398 (2017).

[26] J. M. Pitarke, V. M. Silkin, E. V. Chulkov, and P. M. Echenique, Theory of surface plasmons and surface-plasmon polaritons, Rep. Prog. Phys. **70**, 1 (2007).

[27] R. H. Ritchie and R. E. Wilems, Photon-plasmon interaction in a nonuniform electron gas. I, Phys. Rev. **178**, 372 (1969).

[28] E. G. Harris, *A Pedestrian Approach to Quantum Field Theory* (Courier Corporation, New York City, New York, 2014).

[29] M. Maggiore, *A Modern Introduction to Quantum Field Theory*, Vol.12 (Oxford University Press, New York, 2005).

[30] R. H. Ritchie, J. C. Ashley, and T. L. Ferrell, The interaction of photons with surface plasmons, in *Electromagnetic Surface Modes*, edited by A. D. Boardman (Wiley, Chichester, 1982), Chap. 2.

[31] E. Zeidler, *Quantum Field Theory II: Quantum Electrodynamics* (Springer, Berlin, 2009).

[32] Y. Hadad, J. C. Soric, and A. Alu, Breaking temporal symmetries for emission and absorption, Proc. Natl. Acad. Sci. U.S.A. **113**, 3471 (2016).

[33] D. Sen, A. N. Basu, and S. Sengupta, The difference between the classical and quantum mechanical definitions of scattering cross sections and the problem of the classical limit, Phys. Lett. A **184**, 159 (1994).

[34] D. Sen, A. N. Basu, and S. Sengupta, Classical limit of scattering in quantum mechanics—A general approach, Pramana **48**, 799 (1997).

[35] B. Mandal, A. Semenov, and D. Babikov, Calculations of differential cross sections using mixed quantum/classical theory of inelastic scattering, J. Phys. Chem. A **122**, 6157 (2018).

[36] I. Martínez, J. Andrés, M. F. Groß, Y. Chen, T. Frenzel, V. Laude, M. Kadic, and M. Wegener, Experimental observation of roton-like dispersion relations in metamaterials, Sci. Adv. **7**, eabm2189 (2021).

[37] E. Brunkow, E. R. Jones, H. Batelaan, and T. J. Gay, Femtosecond-laser-induced spin-polarized electron emission from a GaAs tip, Appl. Phys. Lett. **114**, 073502 (2019).

[38] C. Lee, G. Kassier, and R. J. Dwayne Miller, Optical fiber-driven low energy electron gun for ultrafast streak diffraction, Appl. Phys. Lett. **113**, 133502 (2018).

[39] F. Hagelberg, *Magnetism in Carbon Nanostructures* (Cambridge University Press, Cambridge, UK, 2017).

[40] COMSOL Multiphysics [https://www.comsol.com/comsol-multiphysics].

[41] P. B. Johnson and R. W. Christy, Optical constants of the noble metals, Phys. Rev. B **6**, 4370 (1972).

[42] E. D. Palik, *Handbook of Optical Constants of Solids* (Academic Press-Cambridge, Massachusetts, 1997), pp. 749–763.

[43] U. Kreibig and M. Vollmer, *Optical Properties of Metal Clusters*, Vol. 25 (Springer Science & Business Media, Berlin, 2013).

[44] S. K. Doorn, L. Zheng, M. J. O'connell, Y. Zhu, S. Huang, and J. Liu, Raman spectroscopy and imaging of ultralong carbon nanotubes, J. Phys. Chem. B **109**, 3751 (2005).

[45] B. E. Sernelius, *Surface Modes in Physics* (John Wiley & Sons, New York, 2011).

[46] I. S. Gradshteyn and I. M. Ryzhik, *Table of Integrals, Series, and Products* (Academic Press, New York, 2014).

[47] N. N. Lebedev, *Special Functions and Their Applications* (Prentice-Hall, Englewood Cliffs, NJ, 1965).

[48] J. D. Love, Quasi-static modes of oscillation of a cold toroidal plasma, J. Plasma Phys. **14**, 25 (1975).